2016

Development of an Additively Manufactured Microthruster for Nanosatellite Applications

Kevin Russell Gagne
University of Vermont

Development of an Additively Manufactured Microthruster for Nanosatellite Applications

A Thesis Presented

by

Kevin R. Gagne

to

The Faculty of the Graduate College

of

The University of Vermont

In Partial Fulfillment of the Requirements
for the Degree of Master of Science
Specializing in Mechanical Engineering

May, 2016

Defense Date: March 28^{th}, 2016
Thesis Examination Committee:

Darren Hitt, Ph.D., Advisor
Walter Varhue, Ph.D., Chairperson
Dryver Huston, Ph.D.
Cynthia J. Forehand, Ph.D., Dean of Graduate College

Abstract

Next generation small satellites, also known as nanosatellites, have masses significantly lower than traditional satellites. Including the propellant mass, the total mass of a nanosatellite is often in the range of 1 to 4 kg. These satellites are being developed for numerous applications related to research, defense, and industry. Since their popularity began in the early 2000's, limitations on the downscaling of propulsion systems has proven to be problematic. Due to this, the vast majority of nanosatellite missions have limited lifespans of 90-120 days in low Earth orbit before they reenter the Earth's atmosphere. Although satellites on this scale have little available space for instrumentation, the development in the fields of microsensors, microelectronics, micromachinery, and microfluidics has increased the capabilities of small satellites tremendously.

With limited options for primary propulsion and attitude control, nanosatellites would benefit greatly from the development of an inexpensive and easily implemented propulsion system. This work focuses on the development of an additively manufactured chemical propulsion system suitable for nanosatellite primary propulsion and attitude control. The availability of such a propulsion system would allow for new nanosatellite mission concepts, such as deep space exploration, maneuvering in low gravity environments, and formation flying.

Experimental methods were used to develop a dual mode microthruster design which can operate in either low impulse, pseudo-monopropellant mode, or high impulse, bipropellant mode. Through the use of a homogeneous catalysis scheme for gas generation, nontoxic propellants are used to produce varying levels of thrust suitable for application in nanosatellite propulsion. The use of relatively benign propellants results in a system which is safe and inexpensive to manufacture, store, transport, and handle. In addition to these advantages, the majority of the propulsion system, including propellant storage, piping, manifolding, reaction chambers, and nozzles can be 3D printed directly into the nanosatellite chassis, further reducing the overall cost of the system.

This work highlights the selection process of propellants, catalysts, and nozzle geometry for the propulsion system. Experiments were performed to determine a viable catalyst solution, validate the gas generation scheme, and validate operation of the system.

Acknowledgements

I would like to thank my advisor, Dr. Darren Hitt, for his support, guidance, and input throughout my time at the University of Vermont.

I would also like to thank Dr. M. Ryan McDevitt for his continual interest in creating quality research, extensive technical knowledge, and for providing valuable insight into the intricate workings of the device.

This work was supported by Vermont NSF EPSCoR Grant #YR4 SBIR 25399 and the Vermont Space Grant Consortium.

This work is dedicated to everyone who has helped and supported me in my endeavor for a Master of Science degree. First and foremost my mother, sister, and Maria. All of whom have been invaluable sources of support and encouragement when I was tired and dispirited.

Along with them, I am indebted to the members of Dr. Hitt's group for providing necessary moral support and interesting conversations throughout the last two years. In alphabetical order, Danielle, David, Jason, and Stephanie. I wish them all the best of luck in the future and hope that they eventually find themselves working in spider free offices with windows and ventilation. Additionally, the members of group lunch must also be recognized for mutual encouragement and regular gripe sessions.

I cannot forget to mention Dr. Roopesh Mathur and Dr. Nivedita Gupta. Without talking with and learning from them, I would likely have pursued a different topic of study for this graduate work. With their help, I was able to realize the enjoyment I found through the study and visualization of fluid dynamics.

Table of Contents

List of Figures

Chapter 1

Introduction

1.1 Nanosatellites

Next generation small satellites, also known as nanosatellites, have significantly lower masses compared to the standard satellites of today. The total mass of a nanosatellite is often in the range of 1 to 4 kg. Although satellites on this scale have limited available space for instrumentation, the continued development in the fields of microsensors, microelectronics, micromachinery, and microfluidics increases the capabilities of small satellites tremendously. Low developmental costs allow these satellites to be created at a fraction of the cost of traditional satellites for numerous applications related to research, defense, and industry.

As instrumentation and payload footprints become smaller, nanosatellite functionality increases. Some recent developments include the incorporation of three-axis spin-stabilization and the addition of image and radio wave field devices. Along with this, the ability to create autonomous nanosatellite missions decreases the overall operational costs associated with many of the traditional satellite missions of the past.

The advantage of low mass and volume also allow a large number of nanosatellites to be delivered to space during a single launch, further reducing the deployment and overall mission expenses [1].

Through the development of nanosatellite components which are inexpensive, reliable, lightweight, and have low power consumption, nanosatellites have gained significant ability to perform many of the same operations traditional satellites have performed. Along with this, the ability to launch large numbers of nanosatellites simultaneously allows for the use of swarm or constellation formations to take many simultaneous measurements from multiple points in space. This provides more accurate and descriptive data than was possible with previous satellite technology. Coupling nanosatellite formations with GPS technology allows the position and attitude of each nanosatellite to be measured and adjusted accurately in Earth's orbit as well as in deep space. Although the measurement technology is currently available for this type of mission, current primary propulsion and attitude control limitations are hindering its implementation [2, 1].

To date, the low cost of nanosatellite missions has allowed many groups which lack the funding of large space programs with the ability to contribute to space exploration. Cost reductions of nanosatellite planetary missions have dropped the overall cost by an order of magnitude compared to traditional satellites. In the past, typical planetary missions with traditional satellites have often been in the range of hundreds of millions or billions of dollars. These same missions, performed with nanosatellites, now have overall costs of less than ten million dollars [3]. This improvement has allowed space programs in countries with little funding to take on a larger role in space exploration. An example is the Canadian Asteroid Rendezvous And Visit Enabled by Lightsail

(CARAVEL), which is a low cost nanosatallite mission that is easily affordable by the Canadian Space Agency. Without the significantly reduced construction and launch costs, it is unlikely the Canadian Space Agency would be able to have an impact beyond making minor contributions to expensive missions led by much larger space agencies [4].

1.2 CubeSats

The CubeSat project has been an ongoing endeavor since its creation by Prof. Jordi PuigSuari and Prof. Bob Twiggs in 1999. Since then, it has gained immense popularity for the development of nanosatellites for scientific, private, and government payloads [5]. The CubeSat platform offers a low cost alternative to traditional satellites due to their low Size, Weight and Power (SWaP). Through standardization of dimensions and launch methods, the overall cost of access to space has been further decreased though the implementation of a common deployment system, called the Poly Picosatellite Orbital Deployer (P-POD) [5]. The P-POD removes the otherwise necessary step of integration of the CubeSat into the launch vehicle by providing a standard platform for CubeSat deployment. In total, each P-POD has the ability to carry up to three 1 unit CubeSats.

The dimensions of a CubeSat unit is 10 cm x 10 cm x 11 cm with a maximum mass of 1.33 kg per unit. Using this design, units can be combined linearly to a maximum of three units. By doing this, CubeSats with larger payloads and subsystems can be designed for deployment via P-POD. The P-POD is shown in Figure 1.1 [6]. The P-POD's dimensions are 13 cm x 16 cm x 40 cm, and can hold a total of three

CubeSat units. Although the P-POD is the current standard for CubeSat deployment, CubeSat deployers have been designed with the ability to deploy both larger numbers of CubeSats as well as CubeSats with dimensions greater than three units. An example is the deployer jointly designed and created by Innovative Solutions In Space (ISIS) and Andrews Space. This deployer has been developed with the ability to launch a total of thirty-five 12 unit CubeSats [7]. The ability to launch large numbers of CubeSats has been demonstrated. In 2014 a total of thirty-three CubeSats were deployed from the International Space Station over a period of 17 days. Twenty-eight of those were for monitoring natural disasters, deforestation, agricultural yields, and other environmental changes with the ability to capture data with a resolution between three and five meters [8].

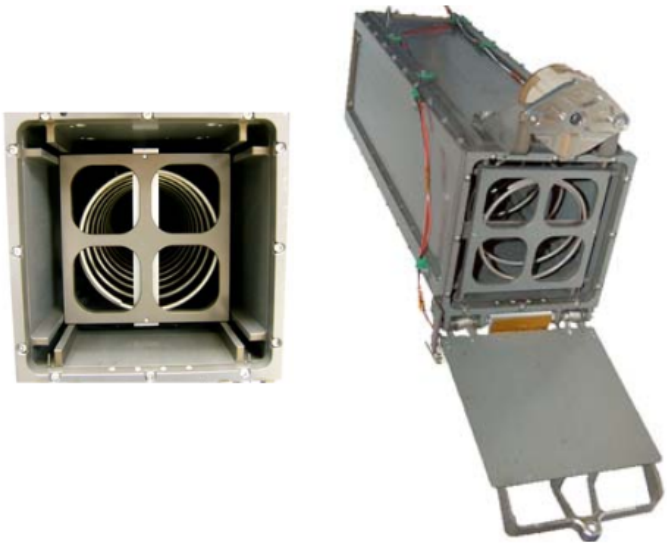

Figure 1.1: The standard Poly Picosatellite Orbital Deployer (P-POD) used for transport and deployment of CubeSats. Reproduced from [5].

Due to their small size, CubeSats were often overlooked or deemed invaluable dur-

ing the early 2000's. However, between the first CubeSat launch in 2003 and the end of 2012, a total of 112 CubeSat missions had been flown. By the end of 2013, another eighty were deployed [6]. Since their debut, CubeSats have grown in popularity for industry, government, and academic applications due to the dramatically decreased construction, mission, and operation costs compared to traditional technology. These same attributes will allow CubeSats to continue to gain popularity in the future as technological advances allow them to perform more complex tasks at substantially decreased cost.

1.3 Nanosatellite Propulsion

Recent advances in fields including additive manufacturing, microfluidics, MicroElectroMechanical Systems (MEMS), low power microelectronics, high efficiency solar cells, and advanced materials all contribute to the development of on-board propulsion systems for the CubeSat platform. Incorporating these advances, future CubeSats could enable scientific missions that would be impossible or financially imprudent using traditional satellites. The addition of propulsion systems would provide CubeSats with the ability to incorporate maneuvers allowing for extended mission lifetimes provided by drag make-up, increased ability for attitude control, the ability to perform proximity operations, and the ability to de-orbit [9].

In the near future, the NASA CubeSat Launch Initiative (CSLI) plans on providing over 100 CubeSats with low cost access to space for research purposes. These CubeSats will be developed by both the United States government and non-profit organizations. Without on-board propulsion systems, these missions are expected to

have a lifespan of approximately 90 to 120 days before they fall to earth and burn up in the atmosphere [10]. However, through the integration of propulsion systems, the total lifetime of missions similar to these could be greatly extended for periods limited only by the total on-board fuel. Extended CubeSat missions will provide researchers with the ability to collect more data without the cost of launching and deploying additional CubeSats.

Figure 1.2: Two of 28 CubeSats deployed as part of a CubeSat constellation called Flock 1 from the International Space Station in February 2014. These CubeSats did not have propulsion systems and were expected to re-enter after three to five months. Reproduced from [11].

There are many types of CubeSat propulsion systems currently in development such as solar sails, electrodynamic tethers, ion electrospray, miniaturized Hall thrusters, solid rocket motors, liquid chemical thrusters, cold gas thrusters, and pulsed plasma thrusters [12]. While many of these technologies offer great promise, currently the high cost of manufacturing coupled with the need for technological advancements in electric power generation and storage, thermal management, and power processing units makes these systems inviable. A reliable, low-cost, easily manufactured

propulsion system is necessary for CubeSat propulsion to be widely implemented.

Among the most appealing of the propulsion technologies in development are chemical propulsion systems. The combination of simplicity, reliability, and low power requirements makes them an attractive choice for CubeSat propulsion. Liquid propulsion systems are of particular interest both as primary propulsion and attitude control, as demonstrated by recent efforts such as the University of Vermont Discrete Monopropellant Microthruster[13] and the ESA-sponsored PRECISE project[35], which both use the catalyzed decomposition of a monopropellant to generate thrust. While these propulsion systems are currently in development, each has reported challenges associated with performance of the catalytic chamber due to scaling effects.

1.4 CubeSat Propulsion Technology

The addition of propulsion systems is a crucial developmental step for the CubeSats platform. Recent growing interest CubeSats has prompted many propulsion projects in academia and industry to create a viable, inexpensive, and easily implemented propulsion system. This advancement would make the CubeSat platform a low cost solution for many missions that may otherwise cost millions of dollars. However, the combination of the low thrust and small footprint required for use in CubeSats results in design difficulties that have yet to be overcome using a method that can be widely implemented.

The development of propulsion systems for small satellites has been an important area of research throughout the world. With the vast number of propulsion systems in development it would be unsuitable to provide a thorough description of each

system in this document. Instead, the survey herein will focus on relevant chemical propulsion systems only.

Chemical propulsion systems are attractive for CubeSats because, unlike electrical or propellantless propulsion, they can provide high thrust for rapid maneuvers. Additionally, the simplicity of chemical systems results in less hardware and decreased chance of failure compared to more complex propulsion alternatives.

Chemical propulsion systems for CubeSats have proven to be problematic in the past due to issues with scale down. Research on the development of microscale converging-diverging nozzles has shown that the scale down increases the importance of viscous effects, plaguing these devices with inefficiencies if designed using the same methods as their larger counterparts. Along with nozzles, the size of other components must be reduced including regulators, valves, filters, pressure transducers, piping, and manifolding in order for the propulsion system to operate properly. These miniaturizations have proven to be a difficult task due to unforeseen scaling issues. In addition to scaling problems, the use of toxic and explosive propellants increases the construction and handling costs of the system dramatically, making the overall cost of a chemical propulsion system which utilizes harsh chemicals too large for organizations with small budgets such as universities.

1.4.1 Monopropellant and Bipropellant Propulsion Systems

Monopropellent thrusters which operate through the decomposition of hydrazine are in development by several organizations including JPL, Areojet Rocketdyne Mi-

cro Aerospace Solutions, the National Cheng Kung University, Tethers Unlimited, Firestar, Vacco, and Busek [9, 14, 15, 16]. Although there are many monopropellant systems in development in industry, academia, and government, the most relevant chemical propulsion systems are briefly described below.

Areojet Rocketdyne has developed three Hydrazine based monopropellant propulsion systems designed for use in 3 U and 6 U CubeSats, these include the MPS-120, MPS-120XW, and the MPS-120XL. Along with these, Areojet Rocketdyne has also developed a line of monopropellant thrusters designed for CubeSats that uses AF-M315E, a green monopropellant. Currently, the MPS-130 is marketed as a green monopropellant propulsion system for CubeSats. However, these propulsion systems are still at the system level laboratory testing stages [17, 16].

Stellar Exploration Inc. developed a micropropulsion system utilizing hydrazine as a monopropellant. It was designed around ease of manufacturing and affordability. The propulsion system has specially designed catalysts, valves, and combustion chambers which power four 1.5 Newton thrusters. In initial testing, incomplete decomposition was observed during operation [18].

The HYDROS Propulsion system, developed by Tethers Unlimited, uses solar power for the on-orbit electrolysis of water to create hydrogen and oxygen. The hydrogen and oxygen is then combusted in a bipropellant thruster. The major advantages of this design include the low pressure storage of water as fuel, high thrust, and high specific impulse. Tethers Unlimited claims 100 Ns of total impulse for each 100 mL of water and that the HYDROS Propulsion System will be available in 2016 [19].

Vacco's green monopropellant propulsion system features four throttable 100 mN

ECAPS ADN thrusters. The system can provide a 1808 Ns total impulse and can be scaled from 0.5 to 1 U total volume. The Mars Cube One (MarCO) CubeSats, currently in construction by NASA's Jet Propulsion Laboratory, will use VACCO propulsion systems for reaction wheel desaturation and trajectory correction maneuvers [20].

Busek's green monopropellant thruster provides 500 mN of thrust and a total delta-V of 130 m/s for a 4 kg CubeSat. The total volume of the system can be packaged in 1 U including the propellant tank, and has a total mass of less than 1.5 kg. It is designed for application in a 3 U CubeSat [21].

Hydrogen peroxide has been examined for use as a monopropellant by several academic and government organizations. At the University of Vermont, a MEMS based device was developed that used micromachined silicon pillars coated with silver for the decomposition of hydrogen peroxide. However, the device suffered from incomplete decomposition of the hydrogen peroxide, which could have been caused by inefficient mixing as well as excessive heat losses. Another design was later created using ruthenium oxide nanorods as the catalyst for hydrogen peroxide decomposition. In this design, incomplete decomposition was also found to be a problem with the nanorod catalyst, most likely due to the hydrophobic surface of the nanorods [22, 13].

In 2007, Kwan, Chen, and Chao developed a hydrogen peroxide microthruster which provided 100 mN of thrust. It was designed as a reaction control system using pure platinum as a catalyst. In 2005, it was determined that the high latent heat of water and hydrogen peroxide reduced the decomposition rate, resulting in decreased performance. However, by 2007 the group had developed an operational device with the ability to produce 182 mN of thrust with a specific impulse of 101 s [23, 24].

In 2014, a liquid monopropellant MEMS thruster was designed, fabricated and tested at the Korea Advanced Institute of Science and Technology. The thruster used a blend of high test hydrogen peroxide and ethanol as fuel and platinum as a heterogeneous catalyst. The measured thrusts were about 40% lower than expected [25].

1.4.2 Alternative Propulsion Systems

Monopropellant and Bipropellant propulsion systems provide high thrust and are often used for maneuvers where rapid change of position is required. However, for missions such as deep space missions where rapid maneuvering is not necessary, alternative chemical, electric, or propellantless propulsion may have attractive benefits over monopropellant or bipropellant propulsion.

Alternative chemical propulsion systems include cold gas thrusters, liquefied gas thrusters, solid rocket motors, and digital microthruster arrays. In cold gas thruster systems, the propellant is stored as a pressurized gas. Liquefied gas thrusters are similar to cold gas thrusters, except the propellant is stored in the liquid phase. neither of these propulsion systems require multiple storage vessels, piping networks, or valves. Due to this, they offer a great simplicity at the cost of performance.

Unlike other forms of chemical propulsion, after ignition solid rocket motors do not consume power during operation. Additionally, they have the ability to offer large thrust values and high accelerations. However, thrust and delta-V cannot be altered during use of solid rocket motors and the motors are single use only. The benefits of solid rocket motors lies in their ability to produce large single bursts of delta-V with low power consumption. Digital microthruster arrays provide single-pulse

units of thrust which are attractive due to their low power consumption and ease of installation. However, there are many challenges associated with digital thruster arrays including, timing, repeatability, torque variance between thruster positions, and the use of valuable wall space that could otherwise be used for solar panels.

Electric propulsion has the advantage of small impulse bits for fine attitude and formation flying control. Along with this, electric propulsion has the ability to supply large delta-V due to its high specific impulse. However, unlike chemical propulsion systems, they cannot offer high thrust for rapid acceleration. Electric propulsion options include pulsed plasma thrusters, vacuum arc thrusters, miniature ion engines, miniature hall thrusters, electrospray thrusters - colloid, electrospray thrusters- FEEP, nanoparticle field extraction thrusters, resistojets, microcavity discharge thrusters.

Propellantless propulsion avoids many of the complexities of the systems previously described. In order to generate force without using propellants, propellantless systems must use electromagnetic fields or sunlight to provide acceleration. The use of propellantless systems imposes strict mission planning difficulties and limitations based on electromagntic fields and the availability of sunlight. Propellantless propulsion options include electromagnetic formation flying, electrodynamic tethers, and solar sails [9].

1.5 Historical Usage of Hydrogen Peroxide Propulsion

Although hydrogen peroxide was first synthesized and identified by Louis Jacques Thenard in 1818, it was not mass produced until 1832. Initially, hydrogen peroxide was used as an external irritant for medical purposes and for bleaching works of art. Only low concentrations were available for sale, and the maximum purity achieved in a laboratory setting was 33%. By 1923, LaPorte began large scale production of 27.5% hydrogen peroxide, used mostly in the textile and pulp and paper industries. As the global usage of hydrogen peroxide increased, the Roessler and Hasslacher Chemical Company and Duffalo Electro-Chemical Company began to produce large volumes of hydrogen peroxide via electrolytic manufacturing with purities as high as 35% [26].

Hydrogen peroxide was not used as a propellant until 1935 when Hellmuth Walter began using 80% hydrogen peroxide for submarine turbine drive systems and assisted takeoff units (ATO). By 1936, Walterwerke, Hellmuth Water's company, had designed an operational 2200 lbf ATO engine as well as a 400 horsepower submarine turbine. Soon after, the German V-2 turbo-pump gas generator was the first time hydrogen peroxide was used for rocket propulsion systems. The design of the V-2 operated by injecting 80% hydrogen peroxide with a potassium permanganate catalyst solution [26].

After World War II, the United States' space program constructed several operational reaction control systems and turbo-pump gas generators utilizing hydrogen peroxide as an energy source. However, by the 1980's, hydrazine had almost com-

pletely replaced hydrogen peroxide in many of these applications for performance reasons. During this time, performance was considered important enough to justify the additional costs associated with hydrazine's environmental, toxicity, and operational hazards. This lead to the almost complete abandonment of hydrogen peroxide propulsion systems by the end of the decade. However, in the 1990's, hydrogen peroxide began to see a rise in interest driven by increased environmental concern and low handling costs [26].

1.6 Advantages of Hydrogen Peroxide

Along with mass limitations for a 1 U and 3 U CubeSat of 1.33 kg and 4 kg respectively, the maximum pressure contained in any component is limited to 1.2 atmospheres. These limitations suggest that an energy dense fuel with a low vapor pressure should be used for CubeSat propulsion. Along with adhering to these criteria, the nontoxic and noncorrosive nature of hydrogen peroxide makes it a promising choice for use in a CubeSat propulsion system.

In comparison to other chemical propellants, such as hydrazine and oxides of nitrogen, high test hydrogen peroxide has low toxicity and is considered a "green" monopropellant. Additionally, the volume specific impulse of 90% hydrogen peroxide is greater than most comparable green propellants currently available. In addition, the chemical products of the decomposition of hydrogen peroxide pose no risk to the integrity of the CubeSat structure or any of its components. The decomposition reaction of hydrogen peroxide is shown below.

$$H_2O_2(l) \rightarrow \frac{1}{2}O_2(g) + H_2O(g)$$

Unlike other promising high-energy green monopropellants such as ADN, HAN, and HNF, the decomposition of hydrogen peroxide results in products with relatively low molecular weight. This is an advantage because the operational temperature of the exhaust gases in hydrogen peroxide thrusters can be maintained much lower than that of other green propellants resulting in decreased materials and manufacturing costs [34]. Due to these characteristics, hydrogen peroxide is a relevant propellant option for CubeSats with a significantly reduced cost of manufacturing, storage, and handling when compared to other "green" fuels on the market today.

1.6.1 Autogenous Pressurization

A significant advantage of using hydrogen peroxide as a propellant is the elimination of a propellant pressurization system. In most chemical propulsion systems, an external system must be used to transport the chemicals from storage to the reaction chamber. This system provides the necessary pressure differential to cause the chemicals to flow through the piping network. Often, additional pressurized gas or pumps are used to provide this pressure.

However, when using hydrogen peroxide an additional pressure source is unnecessary. Similar to other chemical propulsion systems, this system utilizes pressure driven flow for supplying the hydrogen peroxide and catalyst solution to the mixing and reaction chamber. However, instead of an external pressure source, the slow auto-decomposition of the hydrogen peroxide into gaseous oxygen and water while in

storage creates enough pressure to supply the propellants to the system.

This simplification decreases the overall cost, mass, and volume of the propulsion system because the need for pumps or external pressure chambers and pressure regulators is eliminated. Along with this, the pressure during launch can be kept well under the maximum allowable 1.2 atmospheres. After the CubeSat is deployed, the auto-decomposition will allow for operation of the system at higher pressures.

When properly stored, Hydrogen peroxide decomposes at rates well below 1% per year. This rate of decomposition allows the hydrogen peroxide to slowly repressurize the storage vessel as the propellants are consumed during operation of the propulsion system. In addition to this, the storage vessel can easily be designed to withstand higher operating pressures, eliminating the concern for storage vessel failure due to pressure build up.

1.7 Storage and Hazards of Hydrogen Peroxide

Hydrogen peroxide has been commercially manufactured since around 1885. Today, it is used in a verity of applications in industries including medicine, pulp and paper, and propulsion. Billions of pounds of industrial grade hydrogen peroxide are used around the world every year. The massive quantities consumed by industry are typically transported and stored in bulk at concentrations as high as 70% [27].

Although rocket grade hydrogen peroxide has a long history of usage as a propellant, a combination of anecdotal evidence and published negative assessments lead many people to disregard hydrogen peroxide as a viable propulsion solution. A large

portion of these beliefs are based on the negative characterizations provided in popular propulsion textbooks such as *Ignition* by Clark. Books like these provide the reader with a strong bias against hydrogen peroxide by drawing attention to the dangers and storage instabilities of hydrogen peroxide while downplaying those of other fuels[28].

1.7.1 Storage Capabilities

Typical long term ground storage scenarios for rocket propellants occur before the construction of a propulsion system as well as after a propulsion system is charged with propellant but not used immediately. Along with these, a charged propulsion system may sit dormant for long periods before launch or may only be used intermittently during a mission for orbital maneuvers or station keeping. These situations require that the propellant is stable for long periods of time. In satellite and spacecraft applications, propellants must be able to be stored in closed, pressurized vessels for as long as 10 years or more without losing the ability to function properly [29].

Hydrogen peroxide's history of usage as an industrial chemical as well as a propellant has proven that it is a viable chemical for long term storage. Sealed storage on-board spacecraft has been demonstrated for periods as long as 5 years, starting with relatively impure hydrogen peroxide compared to today's standards. At the FMC Corporation, a single drum of 90% hydrogen peroxide was stored for over 17 years. After 17 years of storage, the concentration of the hydrogen peroxide was measured to be 84%, a 0.4% average decrease in concentration per year. The normal rate of decomposition for commercial grade hydrogen peroxide using chemically compatible materials is less than 1% per year [29, 27, 28].

Stability of hydrogen peroxide increases with concentration. Although this seems counterintuitive, higher concentrations of hydrogen peroxide have the slowest decomposition rate. Due to the instabilities which develop when impurities are introduced, hydrogen peroxide becomes increasingly unstable as it decomposes causing the concentration of water in the mixture to rise. Today, the technology to produce up to 99% hydrogen peroxide has been developed and proven both safe and economical on the pilot scale. With the ability to produce a high purity product, the long term storability of hydrogen peroxide is increased dramatically compared to 85-90% hydrogen peroxide which has historically been used for propulsion. Along with the improvements in hydrogen peroxide manufacturing, material compatibility has been studied extensively. By determining which alloys slow the auto-decomposition of hydrogen peroxide, storage has become safer and more reliable than ever before. Research suggests that the overall storable lifespan of hydrogen peroxide has increased by a factor between 2 and 10 since 1965 and will continue to increase with future developments [29, 27].

1.7.2 Detonation Risk

Liquid hydrogen peroxide is non flammable. However, the formation of hazardous explosive vapors in atmospheric conditions and temperatures above about 121 degrees Celsius is possible. At this temperature, the vapor pressure of hydrogen peroxide is high enough to exceed the lower explosive limit when mixed with the Earth's atmosphere. However, below this temperature high purity hydrogen peroxide can be stored safely without the risk of explosion caused by flammable vapors [27].

Condensed phase hydrogen peroxide has proven to be stable. Even when boiling

at atmospheric pressure, the liquid phase does not pose a risk of detonation. Although it is not likely to occur in a natural situation, high test hydrogen peroxide has been forced to explode in a laboratory setting. In a recent examination of literature surrounding the explosively of liquid hydrogen peroxide, Solvay Interlox concluded that an adjacent detonation is necessary to provide significant energy to initiate an explosion in liquid hydrogen peroxide. These conclusions were based on several experiments which showed that along with elevated temperatures, a No. 8 detonator with a 50 gram booster charge was necessary to induce a high test hydrogen peroxide explosion. However, these high temperatures and pressures are not likely to occur in standard storage or usage situations. In addition, it is extremely unlikely that vapor phase explosions can cause liquid phase detonations [27].

1.7.3 Toxicity Risk

Hydrogen peroxide is a naturally occurring chemical that is considered a cytotoxic agent. However, it is produced by the human body and can be found at low concentrations in urine as well as exhaled air. In the human body, hydrogen peroxide does not readily oxidize most biological molecules. Along with this, it is present at levels high enough to be detected in drinking water, rain water, sea water, and is a normal part of a human's diet [30].

When compared to hydrazine, the toxicity and handling characteristics are less hazardous or equivalent for hydrogen peroxide. Hydrogen peroxide's low vapor pressure presents little risk of inhalation. Due to this, high concentrations of dangerous vapors are unlikely at normal storage temperatures. Effects of the vapors are generally low at ambient temperatures and can be almost completely avoided through

proper handling techniques and personal protective equipment. Since the beginning of commercial production of hydrogen peroxide in the early twentieth century, there has been little evidence of toxicity on workers or surrounding communities [27, 28].

1.7.4 Safety Conclusions

When handled and stored properly, hydrogen peroxide poses a low risk of detonation, fire, and toxicity. Using modern storage methods, materials, and high purity hydrogen peroxide, decomposition can be maintained well below 1% per year. Hydrogen peroxide has long term stability in storage, and has proven throughout the last 100 years of commercial high purity production that it can be handled safely. Due to the low risk of storage and handling, hydrogen peroxide offers a low operating cost alternative to the toxic monopropellents which are often used today [27, 28].

1.8 Recent Relevant Work

Hydrogen peroxide decomposition generates high temperature gas which can be used as a working fluid for many applications such as reaction control, primary propulsion, and auxiliary power [31]. Due to this, the catalytic decomposition of hydrogen peroxide has been studied intensely since its first propulsion applications in the 1930's [26].

Catalysis of the decomposition of hydrogen peroxide can be achieved through either heterogeneous or homogeneous catalysis. In heterogeneous catalysis, a catalyst that is a different phase initiates the decomposition reaction. This is typically a solid phase catalyst such as platinum or silver. In homogeneous catalysis, the catalyst is

the same phase as the hydrogen peroxide. Due to this, homogeneous catalysts are liquids that are miscible with hydrogen peroxide.

1.8.1 Heterogeneous Catalysis

Heterogeneous catalysis of hydrogen peroxide is generally performed using a solid catalyst in packed columns, beds, or screens. When hydrogen peroxide comes into contact with the surface of the solid catalyst, the decomposition reaction proceeds rapidly creating steam and oxygen as products. Upon contact, the hydrogen peroxide uses the surface properties of the solid catalyst to decrease the activation energy necessary for the reaction to take place. This results in a drastic increase in reaction rate through the alterations of the chemical kinetic properties of the reaction. This is caused by altering the intermediate steps resulting in a lower activation energy pathway for the decomposition reaction.

Heterogeneous catalysis for thrust applications has been used extensively throughout history. Rocket grade, 90%, hydrogen peroxide was first used for attitude control on the X-15 and Mercury spacecraft in the late 1950's. In this design, silver was used as a catalyst. Here, the hydrogen peroxide was pushed through silver plated screens to initiate the decomposition reaction. This process effectively decomposed the hydrogen peroxide. The gaseous reaction products were then sent through a nozzle to provide thrust. In more recent systems, the screen mesh size has been decreased and silver electroplate is used to promote the reaction and increase the performance of the catalyst system [32].

The performance of this type of catalysis depends on the available catalytic surface area. Due to this, dense screens are preferable for increased reaction rate. However,

flow resistance also increases as the screen density is increased resulting in the need for increased pressure drop to achieve high flow rates through the catalytic system. Pressure drop over these screens is significant and can be as high as 80 to 90 PSI [32].

In heterogeneous catalysis systems, the liquid hydrogen peroxide must contact the surface of the screens in order to decompose catalytically. There are three types of catalyst degradation that can render a surface catalyst ineffective. First, non-volatile materials dissolved in the hydrogen peroxide, such as contamination during production, are left behind as deposits on the surface of the catalyst. This makes it impossible for the hydrogen peroxide to contact the contaminated areas, reducing the effective catalytic area. Second, stabilizers used to prolong the life of the hydrogen peroxide while in storage can also poison the catalyst by disabling its ability to catalyze the decomposition in the same way that it stops the decomposition during storage. Third, a combination of pressure and thermal stresses can cause mechanical damage to the catalyst resulting in clogging or channeling [28].

There are several MEMS-based monopropellant propulsion systems in development which utilize heterogeneous catalysis. Most notably, the PRECISE (chemical μPRopulsion for an Efficient and accurate Control of Satellites for Space Exploration) system in development by the European Space Agency and the MEMS-based microthruster developed at the University of Vermont. Design of catalyst beds on such small scales has proven to be problematic for both systems. Not only do manufacturing techniques need to be taken into consideration, microfluidic effects create unexpected fluid flow patterns on the micro scale [22, 35].

PRECISE was designed to operate in the thrust range of 1-10 mN for application

in accurate attitude control systems on small satellites. In order to achieve thrust in this range, it was necessary to supply approximately 6 mg/s of hydrazine to the catalyst bed. During the development of PRECISE, several heterogeneous catalysis drawbacks were recognized on the micro propulsion scale. These included, significantly increased pressure drop, the need to account for microfluidic effects, and that grain-based catalysts are not viable on this scale. In 2014, several different microcatalyst designs were being considered. Through the variation of coatings and geometries inside the catalyst bed, researchers will try to develop a catalyst that is thermally and mechanically stable [35].

At the University of Vermont, a thruster design relying on a MEMS-based catalyst bed was designed and tested. The catalyst bed used an etched diamond pillar geometry for the catalytic chamber design which was coated with high purity (>99.999%) silver. The catalyst bed geometries tested can be seen in Figure 1.3. During test firings, the catalyst chamber design did not achieved complete decomposition of the hydrogen peroxide [22].

A second catalyst chamber design was later tested at the University of Vermont. Unlike the first catalyst bed, this system utilized self-assembled ruthenium oxide nanorods which were grown on the surfaces of the reaction chamber's walls. Verification of the ruthenium oxide nanorods was performed by scanning electron microscope which confirmed that the growing technique yielded a uniform density nanorod coating in a pillar configuration to increase the effective surface area of the catalyst. The pillar configuration is shown in Figure 1.4 [13].

During operational testing, complete decomposition of the hydrogen peroxide was not achieved accross the nanorod catalyst bed. Additionally, the side of the catalyst

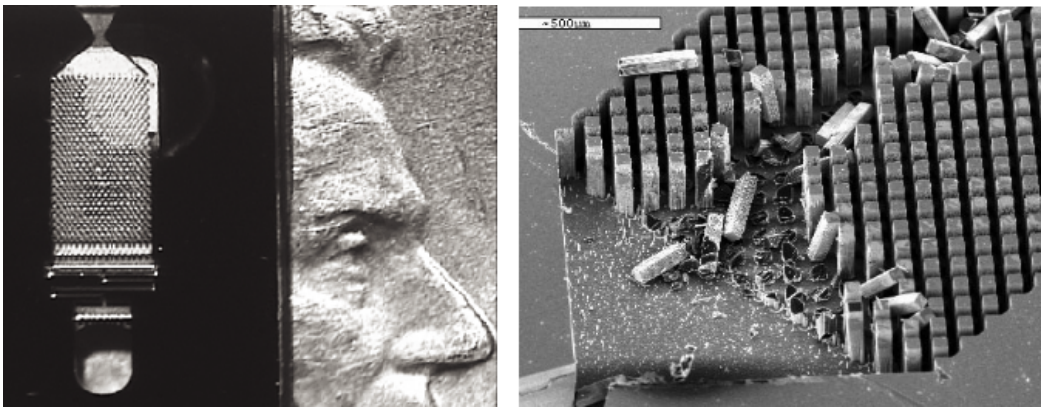

Figure 1.3: Left: A photograph of the MEMS microthruster with a silver coated catalyst bed in comparison to a US penny, developed by the Goddard Space Flight Center with help from the University of Vermont. Right: A close up view of the silver coated diamond pillar catalyst bed, some of the pillars in the catalyst bed have been damaged to show the entire pillar structure. Reproduced from [22].

bed with the lowest density of nanorods showed the greatest gas production. This was an unexpected result as reaction rate was thought to be related to catalyst surface area. It was concluded that due to surface tension effects, the nanorods acted as a non-wetting surface. The hydrophobic nature of the ruthenium oxide nanorods greatly reduced the contact area between the nanorods and hydrogen peroxide, making them ineffective as catalysts [13].

1.8.2 Homogeneous Catalysis

Homogeneous catalysis occurs when hydrogen peroxide is mixed with a liquid phase catalyst. Upon mixing with the catalyst the hydrogen peroxide decomposes, forming gaseous steam and oxygen.

Homogeneous methods of catalysis have been used since the beginnings of experimentation with hydrogen peroxide for propulsion applications. Notably, the Helmuth

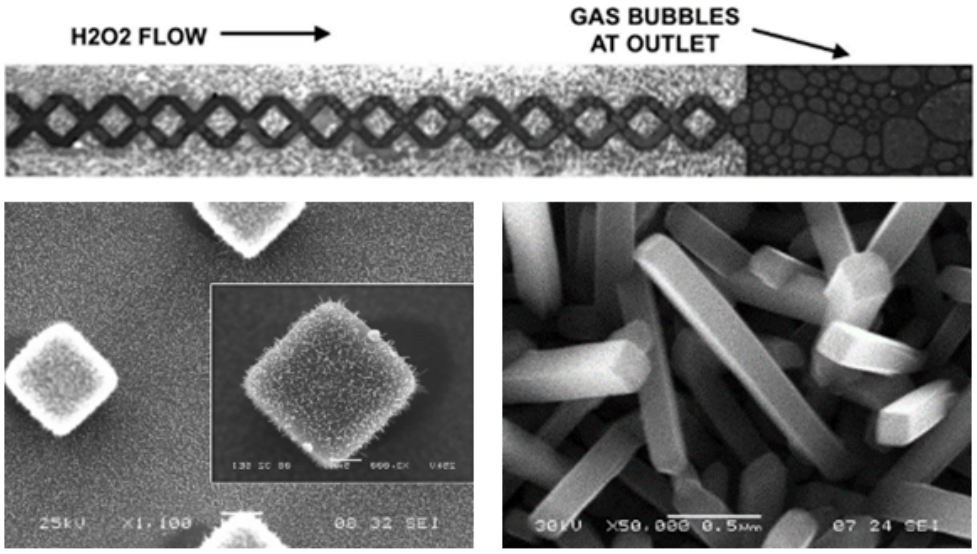

Figure 1.4: Top: Gas bubbles at channel outlet show incomplete decomposition of hydrogen peroxide over catalyst bed. Bottom Left: Scanning electron microscope (SEM) photograph of deposited Ruthenium Oxide nanorod catalyst. Bottom Right: High magnification SEM photograph of Ruthenium Oxide nanorod catalyst layer. Reproduced from [13].

Walter and Heinkel HE176 aircraft, flown in 1938, and later the V2 ballistic missile. Both of these devices used aqueous solutions of calcium permanganate as a catalyst for hydrogen peroxide decomposition. In these devices, the catalyst solution was fed in parallel with hydrogen peroxide into a reaction chamber where they mixed causing the decomposition reaction to take place [32].

In a previous effort at the University of Vermont, a novel method for decomposing a monopropellant on the micro scale was proposed [38]. In this scheme, shown in Figure 1.5, the monopropellant and an aqueous catalyst were fed into a mixing chamber in microscale slugging flow to initiate the decomposition of hydrogen peroxide. The slugging flow increased mixing in the reaction chamber through the natural internal circulation of the slugs. The gaseous reaction products were then ejected through a

converging-diverging nozzle. This system offers a number of advantages over a traditional heterogeneous catalytic bed, including reduced pressure drop, lack of catalyst bed fouling, and improved performance. Perhaps the most important advantage, however, is that eliminating the catalyst bed opens the potential for a propulsion system where the majority of the components are additively manufactured.

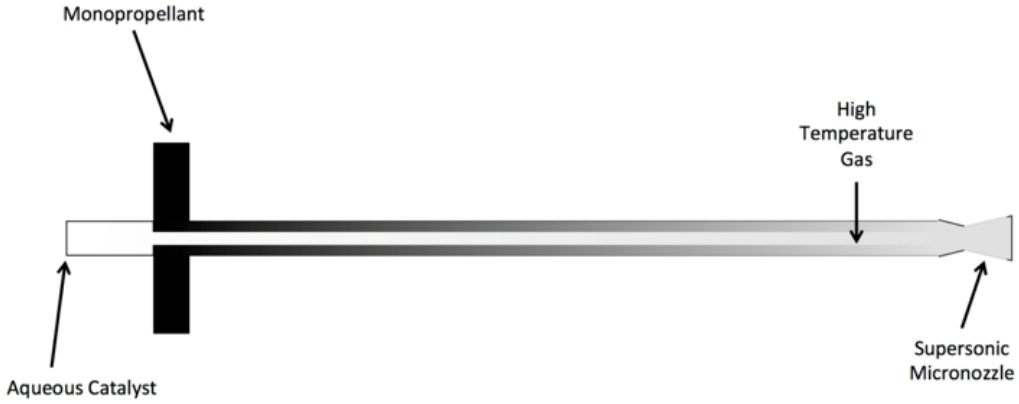

Figure 1.5: Schematic of the homogeneous catalysis concept. The monopropellant is brought into contact with an aqueous catalyst in a specially designed mixing chamber, which results in rapid, exothermic decomposition. The resulting products are vaporized and ejected through a converging-diverging nozzle to generate thrust. Reproduced from [38].

1.9 Description of Work

The goal of this project is to create an operational chemical propulsion system which can be additively manufactured and incorporated directly into a CubeSat chassis. The propulsion system design takes into account the necessary thrust, impulse bit, specific impulse, and total delta-V for use as a CubeSat primary propulsion and attitude control system. The resulting propulsion system is designed to be inexpensive while maintaining long term reliability.

The work described herein includes proof of concept experimentation along with the theoretical and experimental selections of catalyst, catalyst solvent, material of construction, and manufacturing method. Finally, the operation of the system is verified through temperature measurements at the exit plane of the nozzle and thermal images of the exhaust gas plume. The results of this study support the development of an additively manufactured thruster that is suitable for both attitude control and primary propulsion for a CubeSat-class satellite.

Chapter 2

Advantages of Homogeneous Catalysis

Beyond the ability to additively manufacture the system, the use of homogeneous catalysis offers several other advantages over heterogeneous catalysis. One of the foremost advantages of homogeneous catalysis is the ability to vary the ratio of catalyst solution to hydrogen peroxide, resulting in different properties of the nozzle exhaust fluid and the ability to vary thrust and impulse bit without altering the propulsion system. This can be exploited though the careful selection of catalyst and catalyst solvent resulting in a substantial increase in the propulsion system's versatility.

Along with this, the continuous replenishment of catalyst insures that catalyst degradation or poisoning will not cause reliability issues as the spacecraft ages. This, combined with the autogenous pressurization of the system resulting from the slow auto-decomposition of hydrogen peroxide while in storage, makes this system ideal for long missions which require varying thrust levels and impulse bits.

2.1 Homogeneous Catalysis Process

Similar to the homogeneous catalysis propulsion systems produced in the past, the propulsion system described in this work operates in three stages. These three stages are storage, mixing and reaction, and expulsion. A diagram outlining the principle stages of operation is shown in Figure 2.1.

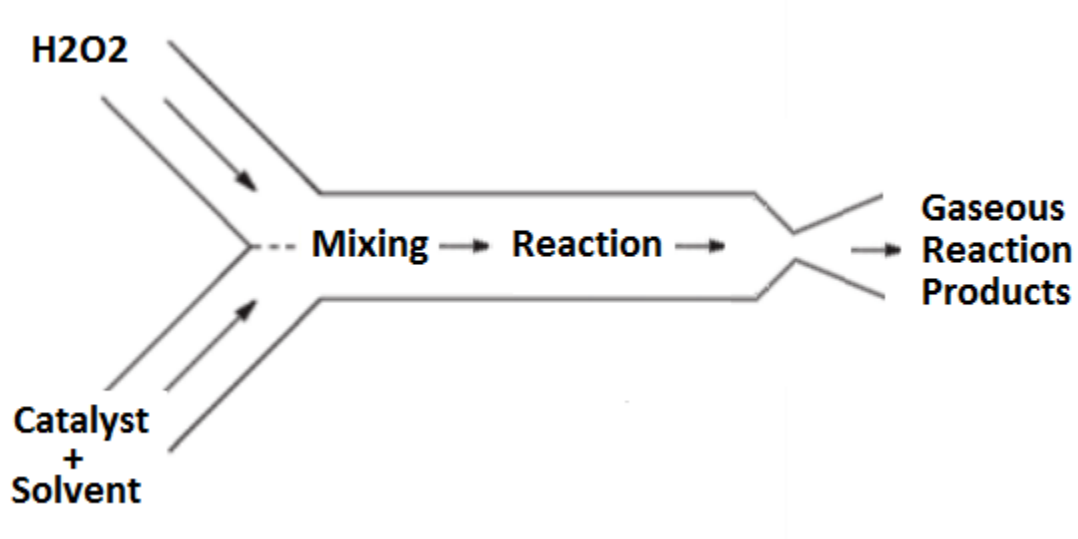

Figure 2.1: This drawing shows the general principle of homogeneous catalysis and how it is applied in the system outlined in this paper. High test hydrogen peroxide and catalyst are both fed into a mixing chamber from their respective storage vessels. In the mixing and reaction chamber the chemical reaction takes place, producing gaseous reaction products. The gases are then expelled through a converging-diverging nozzle.

In the storage stage, the catalyst solution and hydrogen peroxide are both stored separately in chemically compatible vessels. In this system, the storage vessels will be pressurized by the slow auto-decomposition of hydrogen peroxide, resulting in a pressure increase in the storage vessels without the need for an external pressure source.

The second stage, mixing and reaction, occurs when the hydrogen peroxide and catalyst solutions are allowed to flow into the mixing and reaction chamber of the thruster. Here, the catalyst solution is mixed with the hydrogen peroxide resulting in a fast decomposition reaction. This reaction produces steam, oxygen, and heat. The heat released by the decomposition reaction vaporizes the catalyst solvent. Due to the high temperature created by the decomposition reaction, the catalyst solvent vapors react with the oxygen resulting in a combustion reaction. This second reaction releases additional thermal energy into the flow.

After the reactions have occurred in the mixing and reaction stage, the hot product gases enter the third stage of the propulsion system, the converging-diverging nozzle. The decrease in mass density of the gaseous reaction products compared to the density of the liquid reactants results in substantial pressure increase in the mixing and reaction chamber. This pressure drives the reaction products through the converging-diverging nozzle. Here, the flow is accelerated to supersonic conditions in order to produce thrust.

2.2 Dual Mode Operation

A significant benefit of the homogeneous catalysis process is the ability to operate in two distinct modes, pseudo-monopropellant mode and bipropellant mode. These different modes of operation are achieved by varying the the flow rates of the catalyst solution and hydrogen peroxide. By changing the ratio of catalyst solution to hydrogen peroxide in the mixing and reaction chamber, the resulting thrust and impulse bit can be altered and optimized for specific situations.

At the lowest operational ratio of catalyst solution to hydrogen peroxide, the thrust produced will approach the results of a monopropellant thruster, this is the pseudo-monopropellant mode of operation. Increasing the ratio of catalyst solution to hydrogen peroxide to a stoichiometric ratio allows all of the oxygen produced by the hydrogen peroxide decomposition to be consumed though a combustion reaction with the catalyst solvent. Coupling the combustion of the catalyst solvent with the decomposition of hydrogen peroxide results in a dramatic increase in thrust. This mode of operation is similar to a bipropellant system, and is considered the bipropellant mode of operation.

Dual mode operation allows the thruster to alter its performance through the manipulation the ratio of catalyst solution to hydrogen peroxide, resulting in a change in thrust. Due to this, the propulsion system is suitable for both attitude control and primary propulsion for CubeSat-class satellites. Dual mode operation allows the satellite to have full functionality of a reaction control system as well as a primary propulsion system without the need for two separate propulsion systems.

When the decomposition of hydrogen peroxide is coupled with the combustion of a catalyst solvent, the overall reaction products are carbon dioxide and steam and the total number of gas particles created by the reaction is increased. This, along with an increase in the heat evolved from the chemical process results in larger stagnation pressures and temperatures upstream of the nozzle. The bipropellant mode of the thruster design takes advantage of these properties resulting in an increased thrust and impulse bit. The theoretical differences between pseudo-monopropellant mode and bipropellant mode can be seen in Table 2.1.

When operating in pseudo-monopropellant mode, the energy released approaches

Table 2.1: Operation parameters of high and low impulse modes. I_sp calculations are performed assuming a perfect converging-diverging nozzle, thrust is calculated using flow rates that will produce 50 mN of thrust during low impulse operation, impulse bit is calculated using a 10 ms valve actuation time, and Delta-V is calculated for a 3U CubeSat with 1U dedicated to fuel and oxidizer.

	I_{SP} (s)	Thrust (mN)	Impulse Bit (mN*s)	Delta-V (m/s)
High Impulse Mode*	291	112	11.2	986
Low Impulse Mode	161	50	5	574
Percent Difference	57.5	76.5	76.5	52.8

*2-Propanol as catalyst solvent

that of a monopropellant hydrogen peroxide system. In this mode, approximately 586 calories of heat per gram of 85% hydrogen peroxide is released and the adiabatic flame temperature during operation is 886 K [22]. The addition of a stoichiometric ratio of energy-dense solvent significantly increases the energy evolved resulting in an increased adiabatic flame temperature. In comparison to the pseudo-monopropellant mode, the use of a stoichiometric mixture of hexanol and pure hydrogen peroxide results in an energy density of approximately 1050 calories per gram of mixture with an adiabatic flame temperature of 2670 K.

2.3 Application of Dual Mode Operation

Dual mode operation of the propulsion system provides high and low thrust for many applications such as CubeSat maneuvers, station keeping, detumble, reaction wheel desaturation, and attitude control. A major advantage of the system outlined here

is the ability to use the same propellants, piping, and valving for both high and low thrust applications.

2.3.1 Asteroid Exploration

One of the most exciting applications of a dual mode propulsion system is in the ability to use CubeSats for asteroid exploration. Today, there are several current missions using traditional satellites for exploration of asteroids including the Dawn and OSIRIX-REx missions, both lead by NASA, and the Rosetta mission lead by the ESA.

Each of these missions focuses on exploring low gravity targets. Due to the reliable, precise, and low levels of thrust necessary for orbiting these targets, monopropellant propulsion systems are preferred for these applications [36]. However, for missions to targets that call for higher delta-V and specific impulse, bipropellant and solar electric propulsion systems have great advantages over monopropellant systems. Less accessible targets may call for multiple propulsion systems, utilizing high delta-V and high specific impulse propulsion for interplanetary maneuvers, while a second propulsion system is used for attitude control and station keeping while in low gravity orbit.

A dual mode propulsion system designed for the CubeSat platform would provide the necessary propulsion needs to expand CubeSat missions beyond low Earth orbit for many applications such as asteroid flyby or rendezvous. Bipropellant, or high impulse mode, can provide the thrust and specific impulse levels necessary for flyby or rendezvous. During a rendezvous, the pseudo-monopropellant, or low impulse mode, can provide attitude control and delta-V for small position and trajectory adjustments

that need to be made due to the Yarkovsky effect, solar radiation pressure, and variations in the gravitational field of the asteroid.

2.3.2 Formation Flying

CubeSat formation flying requires both primary propulsion and attitude control for maintenance of absolute position of the CubeSat swarm or constellation as well as the relative position of each individual CubeSat in the swarm or constellation. Formations may require both impulsive and low-thrust maneuvers over the course of their mission. Due to the tight volume and mass constraints on CubeSats, the ability to use a single propulsion system for impulsive maneuvers, low-thrust maneuvers, and attitude control is a strong advantage over many other propulsion systems.

2.3.3 Van Allen Belt Travel

High levels of ionizing radiation are trapped in the Van Allen belts caused by the Earth's magnetic field. Here, particles such as electrons, protons, and heavier ions are plentiful. This environment is detrimental to electronic systems on board spacecraft and has the ability to cause many problems including decreased power production by solar arrays, failure of sensitive electronics, and increased background noise in sensors. The high radiation levels in the Van Allen belts have been known to quickly cause damage to satellite electronics resulting in malfunction and failure in as little as a few days. Due to this, total radiation dosages must be reduced when passing though the belts by traveling at high velocity, which decreases the total time spent inside the high radiation regions [37].

The tight mass and volume limitations imposed by the CubeSat specifications limits the additional radiation shielding which can be added for protection. Although electronic and propellantless propulsion systems have high efficiencies, their low levels of thrust make them unable to generate the force necessary to propel CubeSats through the radiation belts quickly. However, chemical propulsion provides the necessary thrust to accelerate small satellites at a high enough rate through the radiation belts to decrease damage. Through the use of the high impulse, bipropellant mode of operation, the homogeneous catalysis system can be used to provide CubeSats with enough thrust to pass through the belts with minimal exposure to harsh radiation, greatly decreasing the shielding necessary to protect sensitive electronics included in the CubeSat's payload. Additionally, the low power consumption of the homogeneous catalysis propulsion system provides it with the ability to operate even if the CubeSat is unable to generate much power due to decreased solar array efficiency.

Chapter 3

Design Considerations

The criteria outlined in the CubeSat Design Specification places strict structural, electrical, operational, and testing requirements on the design and qualification of each CubeSat. By doing this, the CubeSat Program insures the safety of the launch vehicle, primary payload, and other CubeSats on board the P-POD [5]. However, even with strict CubeSat requirements, nearly half of the university-led CubeSat missions which reach orbit fail to achieve mission success. These high failure rates can be attributed to insufficient system-level functional testing prior to launch. Tests such as vibration and operation testing, are expensive and time consuming. Due to this, they are often neglected [6].

The high failure rate associated with CubeSat missions demonstrates the importance of constructing a robust and reliable propulsion system. The propulsion system is a critical part of the CubeSat, if it fails, the CubeSat mission will likely also fail. The design of the propulsion system must have the ability to withstand the high temperatures and pressures without melting, deforming, or cracking due to the thermal and mechanical stresses placed on the material. Along with the material's ability to

withstand these stresses, the manufacturing technique must provide a reliable method for uniform durability throughout the manufactured parts. With the possibility of missions lasting 10 or more years, longevity of the CubeSat chassis and propulsion system are also paramount in importance. The material of construction must also be chemically compatible with the catalyst, catalyst solvent, and hydrogen peroxide in order to avoid possibility of corrosion of the chassis material caused by intimate contact with the propulsion chemicals over the entire mission lifetime. In addition to the material of construction, the chemical propellants must be chosen with long term degradation in mind.

3.1 Additive Manufacturing Considerations

One of the major limitations of additive manufacturing today is the inability to precisely and consistently fabricate complex designs incorporating multiple materials and commercial off the shelf parts. In the past, this limitation has excluded additive manufacturing from being a viable end-to-end fabrication method for CubeSat propulsion technologies. In order to avoid the complications of creating an additively manufactured propulsion system, it is necessary to devise a system which does not have complicated geometries, can be made from a single material, and does not require embedded COTS parts for operation. The homogeneous catalysis scheme described in this work eliminates the need for a complicated catalyst bed resulting in a simplified mixing and reaction chamber geometry and material of construction. Along with this, the use of additively manufactured manifolding allows for COTS valving

to be installed after the chassis has been manufactured. These simplifications of the propulsion system manufacturing process allows for the opportunity to inexpensively additively manufacture the homogeneously catalyzed propulsion system without sacrificing performance.

By incorporating as many parts of the propulsion system into the design of the CubeSat chassis as possible, the number of additional necessary components is significantly decreased. This allows for better use of volume and mass through the integration of the propulsion system into the structural design of the CubeSat. Along with providing more available space, the total number of components and required assembly steps is decreased resulting in a reduced cost of manufacturing. Unlike subtractive manufacturing processes such as milling, turning, cutting, and drilling, there is typically no need for tooling during the additive manufacturing process which further decreases the cost and lead time [39].

There are advantages of additive manufacturing beyond cost, lead time, and mass reduction. By additively manufacturing fluid piping networks, many potential leak paths are eliminated. This occurs because there is no need to plug holes that have been created while drilling the piping networks. Welding and inspection costs are also diminished because the additive manufacturing process does not require welds. This production method results in decreased time for part integration and testing while allowing chassis designs to be optimized for mission specific purposes. The design of simpler systems decreases the number of failure modes, making additively manufactured CubeSats more reliable than their traditionally manufactured counterparts. Overall, the decreased cost and increased performance and reliability make additive manufacturing an attractive option for CubeSats [39, 40].

Preliminary designs of the additively manufactured, homogeneously catalyzed propulsion system have been created by GreenScale Technology, LLC. These initial design drawings of the primary propulsion and reaction control system can be found in Appendix A. The drawings show both systems incorporated into a 3 U CubeSat chassis.

3.1.1 CubeSat Integration

Additive manufacturing has the ability to create cost effective, customized, lightweight CubeSats with high strength and complex components. The combination of small batch sizes and low volume manufacturing makes additive manufacturing an attractive and low cost method of production. The ability to manufacture high quality, high resolution, and metallic parts has provided additive manufacturing the ability to produce mission specific CubeSat designs for a relatively low marginal cost compared to conventional manufacturing techniques.

Additive manufacturing technology is developing rapidly. The ability to fabricate entire electrical and mechanical devices, including full circuits and sensors, will soon be commonplace allowing for many of the onboard systems to be custom printed. With the inclusion of additively manufactured electrical equipment, electrical shorts will be virtually eliminated and CubeSat robustness will be increased dramatically [41, 42].

The first CubeSat with 3D printed parts was launched in November 2013. The design incorporated sensors and printed experiments in order to validate the robustness of the 3D printed parts in the harsh space environment [43]. The RAMPART (RApid prototyped MEMS Propulsion and Radiation Test) CubeSat will likely be the first

CubeSat with a 3D printed chassis flown in space. The RAMPART's chassis is 3D printed from WINDFORM materials that are laser sintered and nickel plated which have been deemed acceptable for use in space through ASME testing. The materials have shown superior strength, brittleness, and thermal properties when compared to polymer materials for additive manufacturing. The RAMPART's launch date, although originally planned for June 2013, has been delayed to a later launch [44].

3.1.2 Material Selection

Unlike CubeSat parts and chassis which have been additively manufactured from polymer or WINDFORM materials, the nozzle and reaction chamber for the homogeneous catalysis propulsion system must withstand high temperatures and pressures. Typical non-metallic additively manufacturing materials would likely melt or burn at these temperatures. The need for temperature resistance suggests that metal alloys with high melting points such titanium or aluminum alloys are more suitable for this application.

Although aluminum alloys have low density and high strength, their melting points are low compared to the adiabatic flame temperatures of the decomposition of hydrogen peroxide when coupled with a combustion reaction. Due to this, additively manufactured aluminum is only an option for pseudo-monopropellant operation. For use in a propulsion system that will operate in bipropellant mode, titanium alloys were chosen for the material of construction because they are less likely to fail due to heat load in the thruster's reaction chamber and nozzle.

The longevity of the material of construction of the CubeSat chassis in a harsh space environment is an important concern for long duration missions. Along with

this, the material must be able to tolerate cyclic heat loads resulting from repeated thruster firings over the lifetime of the CubeSat. The storage vessels must also be capable of withstanding the maximum pressure expected from the autogenous pressurization of the system.

The material of construction will be in intimate contact with both the hydrogen peroxide and catalyst solution for the entire lifetime of the CubeSat. Due to this, long term chemical compatibility between the material of construction and hydrogen peroxide as well as the catalyst and catalyst solvent is imperative. Incompatible materials with hydrogen peroxide may act as catalysts resulting in premature decomposition during storage and catastrophic failure of the storage vessel. Similarly, the corrosive nature of the catalyst could cause significant damage to the material over a short period of time if the storage or piping network in contact with the catalyst is not chemically compatible.

Titanium is an attractive material of construction due to its chemical compatibility, strength, specific weight, and history of usage in aerospace applications. Although there have not been any CubeSats additively manufactured from titanium to date, the Manufacturing Demonstration Facility at Oak Ridge National Laboratory has been focusing on the use of titanium powder in the construction of a 3U CubeSat via an electron beam melting technique. Aerojet Rocketdyne has also began working with additively manufactured titanium as a material for use in CubeSat propulsion [45]. Likewise, NASA has shown interest in additively manufactured titanium parts for aerospace applications which can decrease the cost of some parts by more than 90% while maintaining high quality standards. NASA has created and used additively manufactured complex titanium parts which are exposed to high temperatures

such as headers for rocket engines and "tube-in a tube-in a tube" style parts through the direct metal laser sintering process [46]. Most studies show that the mechanical properties of additively manufactured titanium alloy materials are equal to or exceed their traditionally manufactured counterparts [47].

Along with its mechanical properties and history of usage, titanium's corrosion resistance adds to the attractiveness as a material of construction for this application. Titanium is chemically compatible with hydrogen peroxide, ferric chloride, and ferrous chloride [48]. The chemical compatibility of the materials will allow for long term operation without loss of strength or failure due to corrosion.

3.1.3 Additive Manufacturing Method

In the past, CubeSats have been almost completely manufactured from commercial off the shelf parts. Although this method of production allows for inexpensive, mass produced CubeSat structures, it is not conducive to CubeSat designs that require customized structures due to instrumentation, propulsion, or other subsystem needs. Mission specific CubeSat designs are highly valuable due to the variability between CubeSat missions. The ability to create custom CubeSats with minimum retrofitting and modification saves time and money during the development process. Unlike more traditional manufacturing methods, additive manufacturing has the ability to produce mission specific CubeSat designs at a low cost and with a much smaller lead time. The increased production efficiency caused by additive manufacturing will allow more time and money to be placed on the development and design of the spacecraft subsystems [49].

Additive manufacturing using metallic materials can be accomplished using several

different methods. They are classified into three groups, powder bed, powder feed, and wire feed systems.

Powder bed systems operate by first laying a thin layer of powder on the working surface of the machine. Then, an energy source is used to melt or sinter the powder in the desired shape, forming a thin layer of solid metal. The process is repeated until the thin layers form a three dimensional object. This method produces high resolution features that can contain internal passages while maintaining accurate dimensions. Powder feed systems are similar to powder bed systems. However, powder feed systems use a nozzle to deposit metal powder on the build surface in the desired shape. Then, after the metallic powder has been deposited, a laser is used to melt the thin layer of powder into a solid monolayer. Unlike the powdered systems, wire feed systems use prealloyed wire. The wire is melted using an energy source such as an electron beam, laser beam, or plasma arc. Wire feed systems are typically used for items with large build volumes and often require extensive post print machining [50].

The additive manufacturing method used for a 3D printed thruster, chassis, piping, and manifolding must be chosen to minimize cost while maintaining structural integrity in each part. Based on a survey of commercially available 3D printing techniques, direct metal laser sintering (DMLS) appears to be the most suitable candidate. The combination of high resolution and product quality results in the least amount of post print finishing to provide a smooth nozzle surface.

DMLS is a powder bed system. In this type of system, a metal powder is applied in thin layers to a building platform. Then, a laser is used to fuse the metal particles together in the areas that will make up the part being printed. The remaining metal

powder that was not fused together is removed, and another powder layer is placed on top of the previous metal layer. Through this process, a series of thin layers are fused together to create a three dimensional object. The quality of the part is dependent on the powder material, exposure parameters, inert gas flow, and the temperature on the building platform. Due to the large number of factors that can have a negative effect on part quality, the additive manufacturing process must have camera and diode based monitoring throughout the printing process. By monitoring the manufacturing quality during operation, defects such as porosity, lack of fusion, and rough surfaces can be avoided. The resulting product created by DMLS is a high quality metallic part well suited for application in CubeSats [51].

The laser sintering powder mixture can be composed of a mixture high and low melting point metals. After the liquid metal mixture crystalizes, the high melting point metals add structural integrity while lower melting point metals act as a binder holding the high melting point metals together. Along with this, additives can be used to reduce oxidation, reduce corrosion, or act as a fluxing agent. Prealloyed powders can also be used. Each grain of a prealloyed powder is a mixture of metals and exhibits a zone where solid and liquid exists over a wide temperature range. When using a prealloyed powder, grain boundaries can be formed in the final product resulting in the need for post processing such as furnace post-sintering or hot isostatic pressing [52].

There is little waste created when using DMLS compared to subtractive manufacturing methods such as CNC machining, milling, lathing, or drilling. Along with the significant decrease in waste metal, there are often much shorter turnaround times for additive manufactured parts compared to traditional subtractive manufacturing

methods. Variance in CubeSat design increases the cost of traditionally manufacturing individual, one-off, designs. However, the additive manufacturing process is well suited for customized application reducing the cost of one-off parts. Additive manufacturing also has the ability create low mass parts by printing hollow, strong structures that would not be able to be produced through traditional methods. The strength of the microstructure created during the DMLS process when manufacturing titanium based materials such as Ti-6Al-4V have shown a 50% increase in tensile strength compared to wrought products of the same material [53, 54].

3.2 Catalyst Selection

For optimal performance, the rate of hydrogen peroxide decomposition must generate exhaust gases rapidly and have the ability to maintain high flow rates during steady state operation. Due to this, it is important that the propulsion system design can support high enough reaction rates for sustained operation.

In order for the decomposition of hydrogen peroxide to proceed at a rate fast enough for propulsion, a catalyst is used to lower the activation energy of the reaction. The relationship between reaction rate and activation energy can generally be explained with the Arrhenius equation, shown as Equation 3.1. The Arrhenius equation produces inaccurate results for complex reactions such as this decomposition, but it is useful for understanding what factors may have a significant impact on the reaction kinetics.

$$\kappa = Ae^{\frac{-E_a}{(RT)}} \tag{3.1}$$

Where κ is the rate constant and is directly related to the reaction rate, A is a pre-exponential factor, E_a is the activation energy, R is the universal gas constant, and T is the temperature.

The catalytic decomposition of hydrogen peroxide has been studied extensively. In 1934, Haber and Weiss identified both ferric and ferrous salts as catalysts for a chain and radical decomposition reaction of hydrogen peroxide [55]. In a report published by Sandia National Laboratories, iron compounds were determined to be in the group with the most vigorous hydrogen peroxide decomposition out of all the catalysts studied [56]. Although this decomposition reaction has been studied many times since it was first discovered in 1894 by Henry Fenton, there are no models of the reaction kinetics that can adequately describe the overall reaction rate in a variety of pH, iron ion, and hydrogen peroxide concentrations [33].

To generate thrust, the catalysts used during experimentation must create a rapid decomposition of hydrogen peroxide. Although there are many chemicals and materials that increase the rate of decomposition, few have been extensively researched and documented. Two catalysts were chosen for this application based on the current available literature, those were ferric chloride ($Fe(III)Cl_3$) and ferrous chloride ($Fe(II)Cl_2$). Ferric chloride and ferrous chloride were selected as the homogeneous catalysts for the decomposition reaction for several reasons. The ionic nature of the bonds in these catalysts allow them to readily disassociate into their constituent ions when they are dissolved into polar solvents. This results in a high concentration of iron ions in the catalyst solution, increasing the reaction rate [55, 57, 33]. Along with this, literature suggests that iron salts are among the the highest performing catalysts for hydrogen peroxide decomposition specifically in propulsion system ap-

plications [58, 59].

3.2.1 Catalyst Concentration

The concentration of the catalyst ions is a determining factor in the initial reaction rate which can be described using the second-order kinetic law shown as Equation 3.2.

$$\frac{-d[H_2O_2]}{dt} = \kappa_d[H_2O_2][Fe(III)] \tag{3.2}$$

where κ_d is the second-order rate constant for the reaction, $[H_2O_2]$ is the concentration of hydrogen peroxide, and $[Fe(III)]$ is the concentration of the Fe(III) ion [33]. This shows that there is a strong linear dependence on the concentration of iron ions on the reaction rate. By assuming that the reaction products (H_2O and O_2) are only present in the gaseous phase, the concentration of the iron ions will increase as the reaction proceeds as a result of the decreasing volume of unreacted hydrogen peroxide and catalyst solution. Unlike the concentration of the iron ions, the concentration of hydrogen peroxide will have negligible change over time. This is because the concentration of hydrogen peroxide dependent on the density of the liquid H_2O_2, which has negligible variance with temperature.

Although this model describes the Fe(III) ion, it is likely that the reaction kinetics are similar for the Fe(II) ion. This can be seen in the first two steps of the reaction mechanism described in the literature [33].

$$Fe^{3+} + H_2O_2 \rightarrow Fe^{2+} + HO_2^{\bullet} + H^+$$

$$Fe^{2+} + H_2O_2 \rightarrow Fe^{3+} + {}^{\bullet}OH + OH^{-}$$

The first two steps have a similar mechanism. The first step using Fe(III) as a catalyst produces Fe(II) which is then consumed and produces Fe(III) again as a product of the second step. Due to the similarities, it is likely that the model of the initial kinetics of the reaction suggested for the Fe(III) ion are similar enough to generally describe the reaction kinetics of the Fe(II) ion also.

Although the kinetic equation is a simplified model of the actual chemical kinetics, which have not been completely and accurately modeled to date, the initial reaction kinetics are a valuable concept to understanding what variables will likely effect the overall reaction rate. In this case, the hydrogen peroxide concentration cannot be changed because it depends on the density of the liquid phase hydrogen peroxide. Therefore this model shows that we should expect a larger initial reaction rates by increasing the concentration of the catalyst.

Along with chemical kinetics, increased catalyst concentration also decreases the freezing point of the catalyst solutions. In order for proper operation, neither the catalyst solution nor the hydrogen peroxide can be in the solid phase. Due to this, it is important that the catalyst solution does not freeze at temperatures greater than the freezing point of 90% propellant grade hydrogen peroxide, which is $-10°$C. However, due to the freezing point depression caused by addition of the catalyst to the catalyst solvent, the freezing points of the catalyst solutions are depressed below the freezing point of hydrogen peroxide for each combination of catalyst and solvent of interest, including water.

Minimization of Catalyst Mass

As the reaction proceeds, the total volume of the reactants decreases. The concentration of the catalyst will eventually exceed its solubility limit in the solution. At this point, the excess catalyst ions will precipitate out of solution. The solid precipitate is expected to be carried out of the system through the nozzle along with the gaseous products. This produces the potential hazard of slight geometry changes in the mixing and reaction chamber if the precipitate becomes attached to the walls of these sections instead of flowing out the nozzle as expected.

Catalyst loading may also negatively affect thruster performance through the addition of a second phase. As solid catalyst precipitate passes through the nozzle, performance may be substantially degraded. Thrust reductions of up to 19% have been predicted by the addition of a multiphase component with a volume fraction as small as 0.1% [60].

Along with the potential of system geometry changes and decreased thrust from multi-phase flow, another downside of high catalyst concentrations is the additional mass of the catalyst. On small satellites, the total mass restrictions are tight. It is imperative to minimize the total mass of the system by using the minimum concentration of catalyst necessary to promote complete decomposition of the hydrogen peroxide. This will allow the thrusters to operate properly without unnecessary catalyst mass.

Although increasing the mass fraction of the catalyst may result in an increased rate of reaction, the adverse effects caused by additional mass, multiphase loading, and geometry changes must be considered alongside the reaction rate. The combination of these factors could significantly decrease the overall performance of the

propulsion system if excessive catalyst loading is used. Due to this, only mass fractions of catalyst below 25% were considered for experimentation.

3.3 Solvent Selection

The catalyst solvent was selected based on several criteria including freezing point, viscosity, miscibility with hydrogen peroxide, auto-ignition temperature, the ability to dissolve the catalyst, energy density, adiabatic flame temperature, relative specific impulse, toxicity, and chemical hazards. Although all of these criteria are important considerations, no known chemical meets all of the criteria for an optimal solvent. Due to this, six viable solvents were chosen for experimentation based on predicted and tabulated values of the selection criteria.

The six solvents chosen were water, hexanol, n-hexane, ethanol, methanol, and 2-propanol. These solvents stood out among a list of viable solvents as the most promising based on their chemical and physical properties.

3.3.1 Freezing Point

The freezing point of the catalyst solvent is important for the operation of the propulsion system, a frozen catalyst solution will not flow into the mixing and reaction chamber and will cause a system malfunction. In order for the propulsion system to operate normally, both the hydrogen peroxide and the catalyst solvent must remain in the liquid phase. Due to the environment in space, cold operating temperatures are common especially when the satellite is not in direct sunlight. The freezing point of high test peroxide is approximately -10 degrees Celsius for 85% hydrogen peroxide.

Catalyst solutions were selected that would not freeze at higher temperatures than the hydrogen peroxide.

The freezing points of the pure substances are shown in Table 3.1. However, the addition of catalyst as a solute further depressed the freezing point of each catalyst solution. Due to this, even water which has a freezing point of 0 degrees Celsius when pure will stay in the liquid phase for temperatures lower than -10 degrees Celsius after the addition of the catalyst.

Table 3.1: Pure substance freezing points of the chosen catalyst solvents.

Solvent	Freezing Point of Pure Substance (°C)
Water	0
Hexanol	-48.3
N-Hexane	-95.3
Ethanol	-114
Methanol	-97.6
2-Propanol	-89

3.3.2 Viscosity

The viscosity of the catalyst solvent was considered during the selection process to eliminate solvents which may require large pressure drops to flow into the mixing and reaction chamber. The viscosity is directly related to the pressure drop in the fluid network, as can be seen in the Hagen-Poiseuille equation, shown as Equation 3.3.

$$\Delta P = \frac{8\mu LQ}{\pi r^4} \tag{3.3}$$

Where ΔP is the pressure drop, μ is the dynamic viscosity, L is the length of the

pipe, r is the radius of the pipe, and Q is the volumetric flow rate. The pressure driving the fluid flow of both the hydrogen peroxide and the catalyst solution is supplied by the slow decomposition of the hydrogen peroxide while in storage. Due to this, the pressure drop over the hydrogen peroxide piping network and the catalyst solution piping network will be the same. Although increasing the diameter of the catalyst piping network would allow high viscosity catalyst solvent to be used, piping diameter restrictions are imposed when incorporating the piping network into the CubeSat chassis.

Along with this, mixing the hydrogen peroxide with a high viscosity catalyst solvent would likely call for a more complex mixing scheme. The Reynolds number of a flow is inversely proportional to the viscosity of the fluid, as shown in Equation 3.4.

$$Re = \frac{\rho v L}{\mu} \tag{3.4}$$

where ρ is the density of the fluid, v is the velocity, L is the hydraulic diameter, and μ is the dynamic viscosity. High viscosity catalyst solvents flow with lower Reynolds numbers resulting in more laminar flow, increasing the difficulty of mixing. Due to the fact that the mixing and reaction chamber is already small, the addition of flow with very low Reynolds numbers would likely have a substantial negative impact on mixing and overall performance.

3.3.3 Miscibility with Hydrogen Peroxide

In addition to viscosity, miscibility of the hydrogen peroxide and the catalyst solvent plays an important role in the mixing of the solutions. Highly miscible catalyst solutions promote the decomposition reaction in the mixing and reaction chamber. Mixing is important in the thruster design to disperse the catalyst particles throughout the hydrogen peroxide. The use of an immiscible solvent would cause the decomposition reaction to occur only at the interface of the catalyst solvent and hydrogen peroxide.

Solvents with a range of polarities were chosen for testing based on the rule of thumb that miscible materials have similar intermolecular bond types. Alcohols were chosen as primary candidates due to the hydrogen bond in the alcohol functional group, which is similar to the structure of hydrogen peroxide. The similarity in the structures of ethanol and hydrogen peroxide can be seen in Figure 3.1.

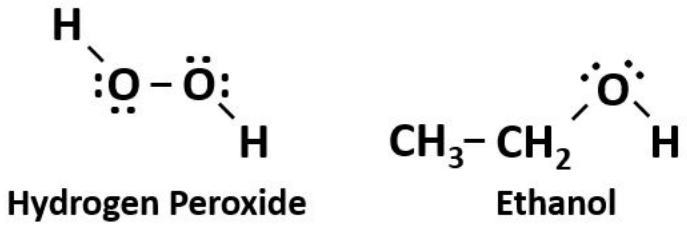

Figure 3.1: Chemical structure of hydrogen peroxide and ethanol. Similarities can be seen between the two structures which lead to high miscibility. The hydrogen peroxide has two hydrogen bonds and the ethanol has a hydrogen bond in the alcohol functional group.

3.3.4 Auto-Ignition Temperature

All of the solvents of interest, except for water, were selected because they are flammable and release a significant amount of energy during combustion. It was important to choose solvents with auto-ignition temperatures higher than typical ambient temperatures experienced by CubeSats during a mission as well as during storage. This requirement insures safety for those working on the device as well as avoiding risk of damage to the launch vehicle and CubeSat during development, construction, storage, launch, and deployment.

Table 3.2: The auto-ignition temperatures of the solvents of interest.

Solvent	Auto-Ignition Temperature (°C)
Water	N/A
Hexanol	293
N-Hexane	223
Ethanol	365
Methanol	470
2-Propanol	399

Solvents with auto-ignition temperatures near the adiabatic flame temperature of the decomposition of hydrogen peroxide (886 K) would not combust during operation of the propulsion system if the hydrogen peroxide or catalyst solvent is fed into the mixing and reaction chamber at low temperatures. This is because the energy released during the decomposition of hydrogen peroxide must heat the entire mixture to the auto-ignition temperature of the solvent in order for the combustion of the solvent to occur. Due to these limitations, only solvents with auto-ignition temperatures between 150 and 500 degrees Celsius were chosen. The auto-ignition temperatures of

the chosen solvents are shown in Table 3.2.

3.3.5 Ability to Dissolve Catalyst

In order to use iron salts to catalyze the decomposition of hydrogen peroxide reaction, the solvent used for catalyst delivery must have the ability to fully dissolve the catalyst at temperatures at or below the lowest operating temperature of the propulsion system.

The minimum operating temperature was chosen as the freezing point of rocket grade hydrogen peroxide, -10 degrees Celsius. It is important that the catalyst solute will not precipitate out of solution above this temperature because operation of the propulsion system with large solid-phase particles could result in reduced flow, total piping blockages, or valve damage. Along with these, precipitation of the catalyst would likely cause the hydrogen peroxide decomposition rate to decrease in the mixing and reaction chamber due to a decrease in iron ion concentration.

Experimental solubility data of the catalysts in each solvent of interest is not currently available. Due to the lack of experimental data, solubility values were predicted using a nonlinear regression model based on 10 chemical descriptors published by Jean-Claude Bradley and Andrew Lang in 2009 [61]. Although the model only predicts solubilities for room temperature solvents, the data was used to eliminate solvents with poor solubility qualities. Solvents with the highest predicted solubility of the catalysts were considered for further experimentation.

3.3.6 Energy Density

When selecting catalyst solvents, the energy density was calculated as the total chemical energy per unit volume of chemical storage. When operating in bipropellant mode, the volumetric ratio of hydrogen peroxide and solvent differs between solvents due to the chemistry of each combustion reaction. By taking into consideration the volumetric ratios of hydrogen peroxide and solvent, the solvent with the highest combined energy density will provide the propulsion system with the highest delta-V per unit of chemical storage space. The energy density was calculated using the formula shown as Equation 3.5.

$$\rho_{Energy} = \frac{\Delta H_{H_2O_2} + \Delta H_{Solvent}}{V_{storage,H_2O_2} + V_{Storage,Solvent}} \tag{3.5}$$

Where ρ_{Energy} is the energy density, $\Delta H_{H_2O_2}$ is the enthalpy released by the hydrogen peroxide during decomposition, $\Delta H_{Solvent}$ is the enthalpy released by the combustion of the solvent, $V_{storage,H_2O_2}$ is the storage volume of the hydrogen peroxide, and $V_{Storage,Solvent}$ is the storage volume of the solvent. This energy density definition is relevant due to the tight volume constraints imposed by the CubeSat platform. In order to have the most compact propulsion system, the total energy density of the storage volume was evaluated. Figure 3.2 shows the calculated energy density based on each solvent of interest.

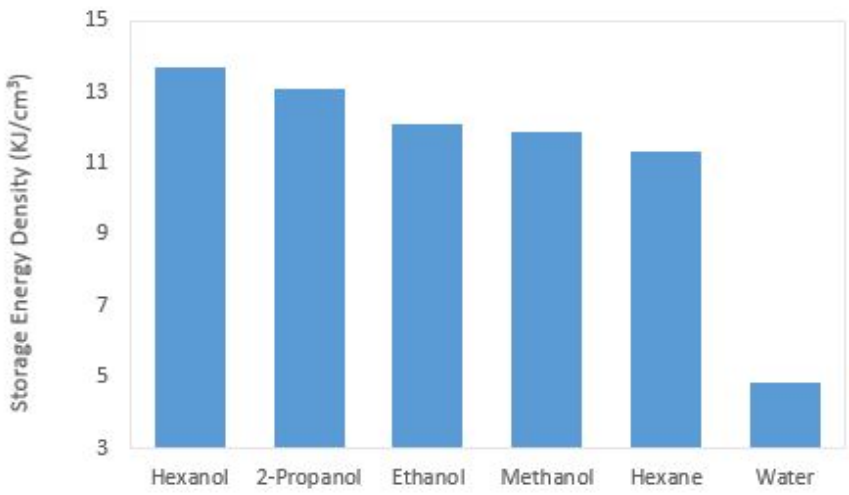

Figure 3.2: The energy density of the stoichiometric ratio of hydrogen peroxide and solvent. Higher energy densities allow for smaller total storage volume leading to decreased system footprint.

3.3.7 Adiabatic Flame Temperature

The adiabatic flame temperature is the theoretical maximum temperature of the product gasses created during the reaction of the hydrogen peroxide and catalyst solution. The addition of water, either as a catalyst solvent or as a result of degradation of the hydrogen peroxide during storage has a great affect on the operation temperature of the propulsion system. The significant impact of water on the operating temperature can be seen in Figure 3.3. Above 0.35 mass fraction of water, the reaction does not evolve enough heat to vaporize all of the water in the product stream. This creates a product stream consisting of saturated steam and water droplets, significantly impacting performance of the nozzle.

Catalyst solvents other than water can be used to increase performance. The replacement of water with a fuel at a stoichiometric ratio of fuel to hydrogen peroxide

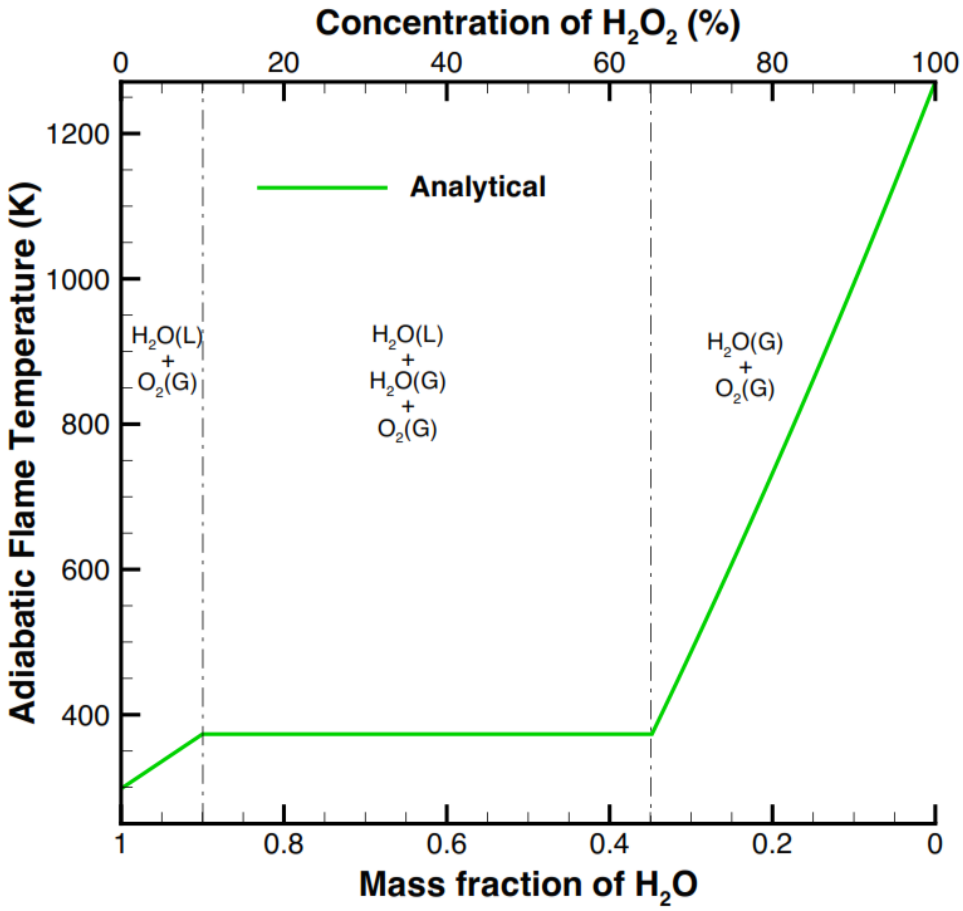

Figure 3.3: Plot of the adiabatic flame temperature verses the mass fraction of water in the mixture. When the mass fraction of water is above 0.35, the reaction products are a mixture of liquid water and saturated steam, causing severe performance degradation.

increases the adiabatic flame temperature of the mixture significantly. This can be seen in Figure 3.4 which shows the adiabatic flame temperatures of the reaction if ethanol, methanol, 2-propanol, hexane, or hexanol are used as the catalytic solvent at stoichiometric ratios.

The use of reactive solvents results in higher adiabatic flame temperatures which increase the thrust and specific impulse resulting in a more efficient propulsion system.

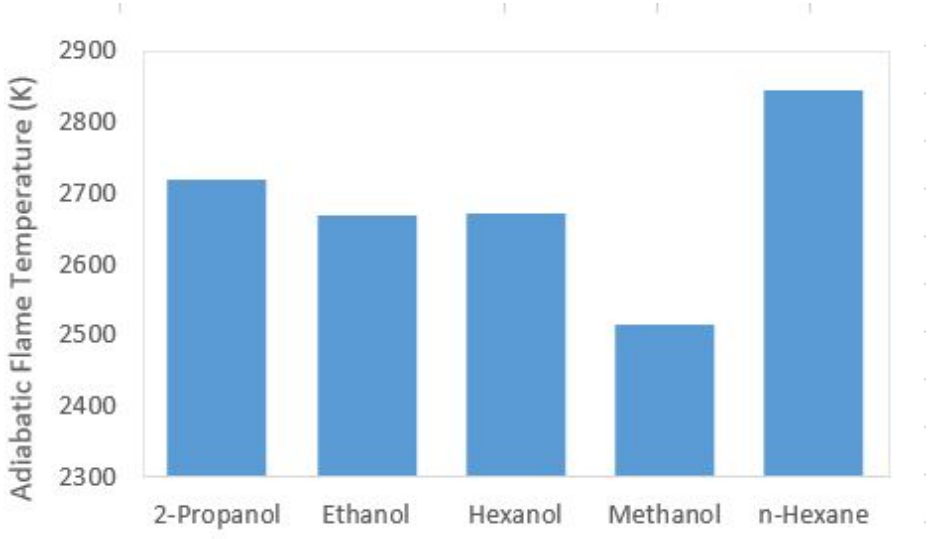

Figure 3.4: Plot of the adiabatic flame temperature of a stoichiometric mixture of hydrogen peroxide and catalyst solvent.

3.3.8 Relative Specific Impulse

Based on the molecular masses and adiabatic flame temperature of the product gasses created in the mixing and reaction chamber, the theoretical relative specific impulse between the various catalyst solvents can be compared. The calculated relative specific impulses for the catalyst solvents chosen are shown in Table 3.3.

Table 3.3 shows the significant increase in specific impulse, thrust, impulse bit, and delta-V achieved by all of the chosen catalyst solvents while operating in bipropellant mode when compared to water. The significant improvement in specific impulse allows smaller volumes of hydrogen peroxide and catalyst solvent to be stored on board for missions where large delta-V is necessary.

Table 3.3: I_{sp}, thrust, impulse bit, and Delta-V in bipropellant mode.

	I_{SP} (s)	Thrust (mN)	Impulse Bit (mN*s)	Delta-V (m/s)
Water	161	50	5	574
2-Propanol	291	112	11.2	986
Ethanol	289	111	11.1	937
Hexanol	296	114	11.4	1000
Methanol	283	109	10.9	858
n-Hexane	297	114	11.4	1018

3.3.9 Toxicity and Chemical Hazards

In order to decrease the overall cost of storage and handling of the propulsion system, only nonhazardous chemicals were considered for use as the catalyst solvent. In an effort to increase environmental friendliness while maintaining high performance, catalyst solvents were chosen that would not pose a significant risk to the environment or the people handling the solvents.

Flammability Hazards

Hexane, ethanol, methanol, 2-propanol, and hexanol are highly flammable and pose a fire hazard when in the presence of open flames and sparks. Due to the fact that the solvents were chosen based on their ability to react at relatively low temperatures, it is not possible to eliminate chemicals that pose flammability hazard. Likewise, solvents with high energy density were chosen because they offer the highest performance for

the CubeSat propulsion system. Similar to many high energy, flammable fuels and solvents used by both industry and the public today, the risk of fire can be minimized with proper handling and storage of the solvents.

Although the solvents do pose a flammability hazard, they were chosen based on their common use in industry. All of the solvents that were tested have a long history of usage in many different industries as fuels and solvents. The common usage of these chemicals shows that when handled properly, they do not pose a substantial fire risk.

Health Hazards

Only solvents that are easily handled and do not pose a significant toxicity hazard were considered for use in the propulsion system. Although the chosen solvents are easily handled, it is still important to use personal protective equipment, maintain adequate ventilation, and have nearby safety showers during handling. By only considering solvents that have a history of safe, large scale industry usage, the chemical hazards in the propulsion system were minimized [62, 63, 64, 65, 66]. Through the process of eliminating chemicals that were extremely toxic, the resulting propulsion system was able to maintain its status as a "green" chemical propulsion system.

3.4 Nozzle Selection

Previous linear micronozzle studies performed at the University of Vermont have focused on micronozzles an order of magnitude smaller than those studied here. In that previous work, a 30° expander was found to offer the best performance for "deep"

nozzles (>100 μm), as it was sufficiently wide to overcome the viscous boundary layer but narrow enough to keep most of the flow in the axial direction [67].

However, in this study, the focus is on slightly larger nozzles which produce more thrust and have higher flow rates. In the numerical study performed on the nozzles at this scale, only the shallowest nozzle (0.25 mm) overlaps with the previous effort. The results from the numerical simulations are shown in Figure 3.5. A detailed description of the computational model and the numerical results can be found in Appendix B.

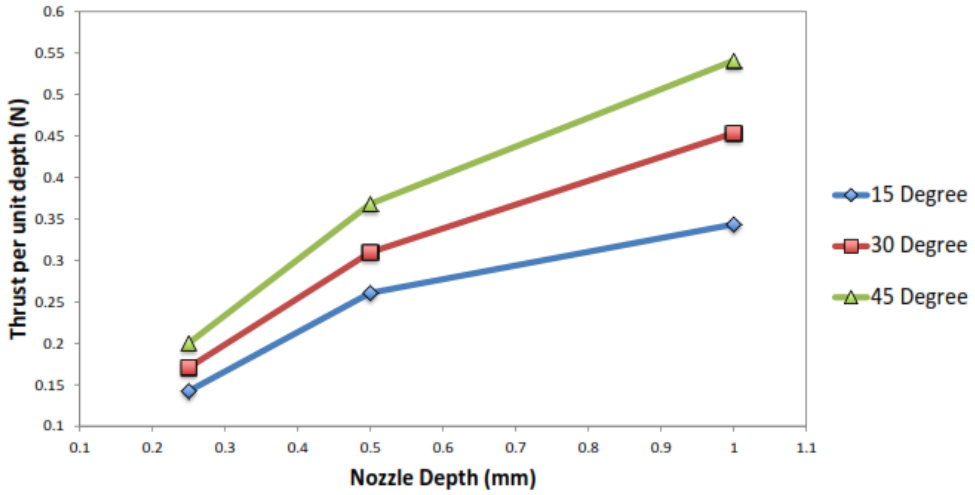

Figure 3.5: The thrust performance per unit depth at Re ≈ 800 for 15°, 30° and 45° expander half-angles at 0.25, 0.50 and 1.00 mm. For the shallowest nozzles, the viscous boundary layer dominates the flowfield, which reduces performance.

Surprisingly, the findings of the computational study, shown in Figure 3.5, performed on this scale indicate that a 45° expander offers the best performance at all depths studied. Based on the previous work, the expectation was that deeper nozzles would suffer less from viscous effects, making the wider nozzle inefficient due to geometric losses. However, the simulation results indicate that viscous effects are still significant enough to warrant a 45° expander over the Reynolds numbers of interest

in this study. Due to the computational results, a nozzle with a 45° expander was used for experimentation.

Chapter 4

Chemical Testing and Analysis

A total of six solvents and two catalysts were selected for experimental testing based on their chemical and physical properties. In order to determine which solvent and catalyst combinations provide the highest performance and reliability in this propulsion system, each combination of solvent and catalyst was tested for solubility and chemical kinetic properties at three concentration levels. The catalysts were tested at concentrations of five, fifteen, and twenty-five weight percent. Due to this, there were a total of thirty-six different combinations of catalyst, catalyst concentration, and solvent.

4.1 Solubility Testing

4.1.1 Background

The determination of solubility of chemical species in a solvent based on chemical structure and chemical descriptors is a difficult problem. Although it has been stud-

ied for decades, computational methods for the determination of solubility still face significant reliability issues. Many of the models that have been developed are solvent specific. Models that are designed with the ability to estimate solubilities in various solvents sacrifice accuracy for the increased solvent inclusivity. Chemical solubility models are typically created for estimation of drug solubility. Due to this, the solvents considered in the majority of models are limited to benign liquids that can be used for pharmaceutical delivery such as water, ethanol, or propylene glycol.

Additionally, estimated solubility values are typically calculated at ambient temperatures of 20-25 degrees Celsius. Although this is acceptable for many applications, the CubeSat propulsion system must operate at temperatures as low as -10 degrees Celsius, far below the prediction temperature. Temperature dependence of solubility is variable between chemical species. As a result, the extrapolation of solubility data to low temperatures has a high risk of inaccuracy and needs to be verified through experimentation.

4.1.2 Experimental Procedure

The solubility of the catalyst in the selected solvents was studied at the approximate freezing point of hydrogen peroxide. To perform this study, each combination of catalyst and solvent were created at concentrations of 5, 15, and 25 weight percent resulting in a total of 36 catalyst solution samples. These concentrations are well below the estimated solubility predicted through the solubility model and were expected to fully dissolve the solutes, even at low temperatures. The samples were placed in a refrigerated area where they were cooled to -10 degrees Celsius and left undisturbed for a minimum of 12 hours. This allowed the samples enough time for any undis-

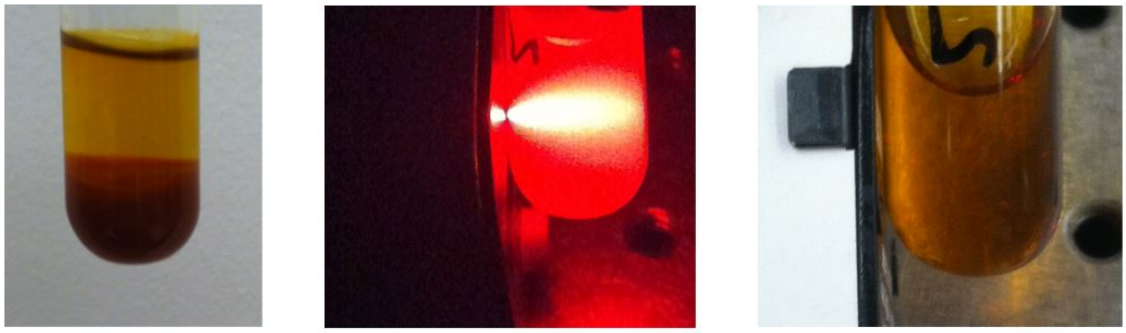

Figure 4.1: Left: An unstable colloid that has settled to the bottom of a test tube. Middle: A stable colloid. Right: A dissolved catalyst, below the solubility limit.

solved solute to settle to the bottom of the test tubes. After the samples were cooled and settled, a visual examination of the samples was performed to determine if the samples were homogeneous.

The samples were then allowed to warm to room temperature. After the samples were at room temperature and there was no condensation on the outside of the test tubes, a laser was used to determine if the solutions were colloidal. The colloid test was performed using a red laser which was pointed through each sample in a dark environment. If the laser scattered, the sample was determined to be colloidal. Homogeneous samples which did not have visible laser scattering were determined to be fully dissolved. Colloidal solutions were allowed to sit, undisturbed, for 12 hours. After 12 hours, the samples were visually inspected for homogeneity. If the solution remained homogeneous, the samples were determined to be stable colloids. If the solution separated, the samples were determined to be unstable colloids. Sample photographs of the solubility test are shown in Figure 4.1.

4.1.3 Experimental Results

Solubility testing resulted in the elimination of 19 of the 36 catalyst solutions of interest. Although predictions for solubility of ferric chloride and ferrous chloride were substantially larger than the concentrations of the solutions which were examined, experimental results showed that actual solubility was lower than predicted for many of the solvents.

Hexane, although predicted to be a viable solvent, did not show any attributes of being a solvent for either the ferric chloride or ferrous chloride. Along with this, five weight percent of either ferric chloride or ferrous chloride in water was not sufficient to depress the freezing points below -10°C. Results of solubility testing are shown in Table 4.1.

Table 4.1: Experimental solubility testing results.

Results of Solubility at -10°C

	$Fe(III)Cl_3$			$Fe(II)Cl_2$		
	5%	15%	25%	5%	15%	25%
Hexane	I	I	I	I	I	I
1-Hexanol	H, NC	H, NC	H, NC	NH, OSL	NH, OSL	NH, OSL
Methanol	H, NC	H, NC	H, NC	NH, NC	H, NC	H, UC
Ethanol	H, NC	H, NC	H, NC	H, NC	H, NC	NH, OSL
2-Propanol	H, NC	H, NC	NH, OSL	NH, OSL	NH, OSL	NH, OSL
Water	Frozen, NC	H, NC	H, NC	Frozen, NC	H, NC	NH, OSL

H=homogeneous NC=noncolloidal, fully dissolved OSL = over solubility limit

NH= not homogeneous UC = unstable colloid I = insoluble

4.2 Drop Testing

4.2.1 Background

Drop testing was used to evaluate the reaction kinetics of each combination of solvent and catalyst that were determined to be viable through solubility testing. A slow decomposition reaction is undesirable because it results in the need for a longer mixing and reaction chamber. In the chemical reactions studied, heat released from the decomposition of hydrogen peroxide causes the combustion of the solvent. Due to this, the rate of decomposition is strongly related to the time between mixing and solvent combustion. Higher decomposition rates provide faster overall reaction times leading to increased propulsion system performance.

In this study, the time between initial contact of the fluids and the onset of a violent reaction is defined as the initial delay time. The initial delay time depends strongly on the heat and mass transfer properties of the system as well as the chemical kinetics [68]. Ideally, the delay could be broken into two contributing parts, delay caused by chemical kinetics, and delay resulting from the heat and mass transfer characteristics of the system. However, mixing limitations prevent the ability to accurately determine the contribution from each of these specific factors.

A minimum chemical reaction delay corresponds to increased system performance by minimizing heat losses from the mixing and reaction chamber resulting in acutal temperatures that are closer to the theoritical adiabatic flame temperature. Along with this, longer initial delays may result in the creation of high concentrations of explosive intermediate species resulting in hard engine starts and decreasing system

reliability. The optimum outcome of drop testing is to find a low toxicity fuel which can be safely and easily stored while still providing short delay and reaction times when mixed with hydrogen peroxide. In previous studies, alcohols were found to be inexpensive, non-toxic, and highly storable, while providing good performance [68, 69].

Although drop testing has historically been the standard method for initial screenings of hypergolic fuel and oxidizer mixtures, it should be noted that there are significant environmental differences between the drop test and the reaction kinetics in the thruster [70]. Mixing is a large determining factor in performance of the thruster being designed in this work. Due to this, it is important to understand that differences in mixing, pressure, and heat transfer between the drop test and use in the thruster will likely cause the reaction to proceed with different kinetics during thruster operation.

4.2.2 Experimental Procedure

Drop testing was performed by mixing 50 microliters of hydrogen peroxide with 50 microliters of catalyst solution inside an additively manufactured aluminum "chalice" shown in Figure 4.2.

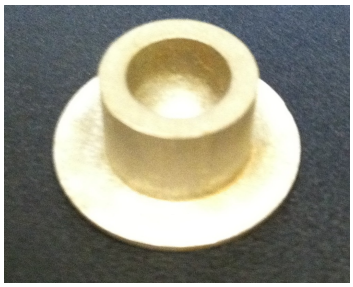

Figure 4.2: Additively manufactured aluminum "chalice" used during the experimental drop tests. The diameter and depth of the "chalice" are both 15.875 mm.

50 microliters of hydrogen peroxide were first placed in the chalice. Then, 50 microliters of the catalyst solution were quickly added to the chalice using a micro-pipette. The reaction was observed and timed. Data was collected pertaining to the length of the initial delay before reaction and the total elapsed time for the substances to react. Incremental photographs of a drop test experiment is shown in Figure 4.3.

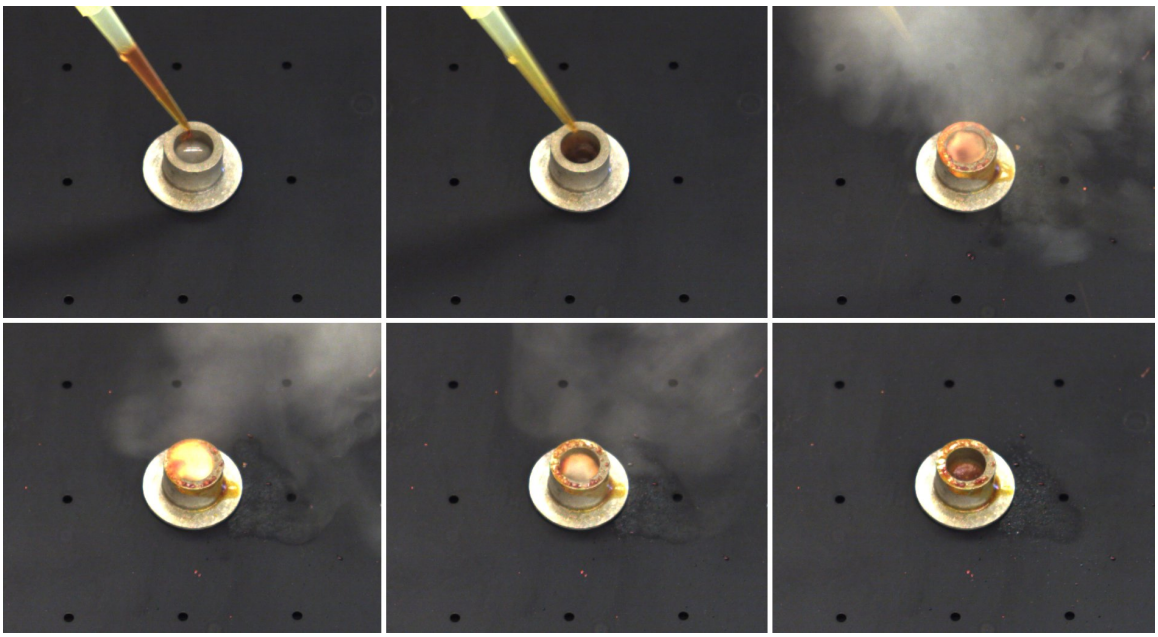

Figure 4.3: Incremental photographs of an experimental trial of a drop test.

During this experiment, each solvent of interest was tested in combination with each catalyst at three levels of concentration. Through this process, every viable combination of solvent, catalyst, and catalyst concentration was examined.

4.2.3 Experimental Results

Each reaction was categorized by delay time and reaction time. The delay times were binned into three levels; no delay, short delay, and long delay. No delay was

defined as having no noticeable delay by the observer. To be placed in the no delay category, the reaction must have begun reacting upon contact of the catalyst solution and hydrogen peroxide. Short delay was defined as a reaction having an initial delay of less than one second after contact between the catalyst solution and the hydrogen peroxide. The long delay category was used for reactions with initial delays greater than one second.

Similarly, the reaction time was categorized into two categories, fast reaction or slow reaction. Fast reactions occurred rapidly, in less than one second, and slow reactions occurred in greater than one second. The results are shown in Table 4.2.

Table 4.2: Observed reactivity of experimental solutions.

Results of Drop Test at 20°C

	$Fe(III)Cl_3$			$Fe(II)Cl_2$		
	5%	15%	25%	5%	15%	25%
Hexane	N/A	N/A	N/A	N/A	N/A	N/A
1-Hexanol	LD, LR	LD, SR	LD, LR	N/A	N/A	N/A
Methanol	LD, LR	ND, FR	ND, FR	LD, LR	ND, FR	ND, FR
Ethanol	ND, LR	SD, SR	ND, FR	LD, LR	ND, FR	N/A
2-Propanol	LD, LR	ND, FR	N/A	N/A	N/A	N/A
Water	ND, SR	ND, SR	ND, FR	ND, LR	ND, SR	ND, LR

ND=No Observed Delay
SD=Delay shorter than 1s
LD=Delay longer than 1s

SR= Reaction less than 1 s
LR = Reaction longer than 1 s
N/A = Not tested due to solubility testing results

4.3 Solubility and Drop Testing Analysis

The results from solubility testing and drop testing were combined to determine which catalyst solutions are viable for the propulsion system. For application in the propulsion system, it is necessary that the catalyst remains dissolved at low temperatures, the solution does not freeze, and that there is a fast decomposition of hydrogen peroxide with no delay. These qualities are necessary for reliable performance in space.

Viable catalyst solutions were selected from the 36 catalyst solutions which underwent solubility and drop testing based on the overall measured performance. Solubility requirements for viable solvents were limited to solutions which were homogeneous, noncolloidal, and unfrozen at -10°C. Along with this, only solutions which had fast decomposition reactions with no observable delay during drop testing were considered. Through this process, the original 36 possible catalyst solutions were further reduced to seven viable catalyst solutions. The results are outlined in Table 4.3, which shows the viable catalyst solvents in white.

Solvents with low concentrations of catalyst, are preferred for propulsion system applications for several reasons. Lower concentrations result in solutions which remain homogeneous at lower temperatures. As temperature decreases the solubility limit of the catalyst in the solvent also decreases. Due to this, low concentrations of catalyst decrease the minimum temperature before solid catalyst crystallizes and precipitates allowing lower operation temperatures and increased reliability for solvents with low catalyst loading. Along with this, the overall mass of the catalyst in the system is

Table 4.3: Observed solubility and reactivity of experimental solutions. Solutions in white cells show high levels of solubility and reaction performance and are promising mixtures for further experimentation.

Results of Solubility at -10C, Overlayed with Drop Test Data

	$Fe(III)Cl_3$			$Fe(II)Cl_2$		
	5%	15%	25%	5%	15%	25%
Hexane	I	I	I	I	I	I
1-Hexanol	H, NC	H, NC	H, NC	NH, OSL	NH, OSL	NH, OSL
Methanol	H, NC	H, NC	H, NC	NH, NC	H, NC	H, UC
Ethanol	H, NC	H, NC	H, NC	H, NC	H, NC	NH, OSL
2-Propanol	H, NC	H, NC	NH, OSL	NH, OSL	NH, OSL	NH, OSL
Water	Frozen, NC	H, NC	H, NC	Frozen, NC	H, NC	NH, OSL

H=homogeneous
NH= not homogeneous
NC=noncolloidal, fully dissolved

UC = unstable colloid
OSL = over solubility limit
I = insoluble

Long delay, slow reaction, or insoluble
short delay followed by fast reaction or unstable colloid
No delay, Fast reaction, Noncolloidal

decreased. At high concentrations of catalyst, the mass of dissolved catalyst can add significant mass to the overall system.

In order to choose which catalyst solutions would offer the best overall performance, the viable catalyst solutions were ranked by expected performance for application in CubeSats. The rank was based on the relative specific impulse(I_{SPR}), catalyst concentration ($Conc_R$), and the relative chemical storage energy density (U_R) of each viable catalyst solution. The formula used to determine the expected performance is shown as Equation 4.1.

$$\text{Expected Performance} = U_R * 5 + I_{SPR} * 5 - Conc_R * 1.5 \tag{4.1}$$

From this, the relative expected performance was determined by normalizing the

expected performance with the highest performing solution, 15% ferric chloride in 2-propanol. The relative expected performance of each catalyst solution is shown in Figure 4.4.

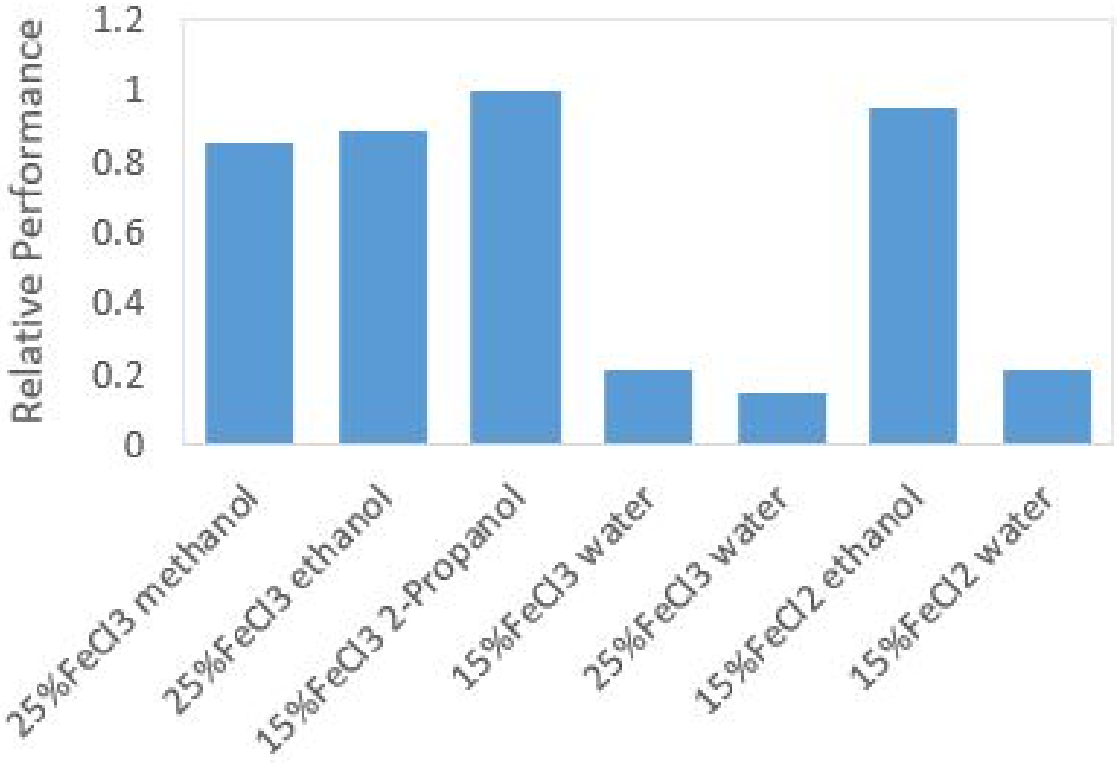

Figure 4.4: The relative expected performance of each solution of interest based on three major performance and reliability characteristics including storage energy density, relative specific impulse, and solute concentration.

Based on this information, 15% ferric chloride in 2-propanol shows the highest expected performance for the propulsion system. This catalyst solution was chosen for further testing based on its performance and reliability characteristics.

Chapter 5

Thruster and System Testing

5.1 Thruster Description

Thruster and system testing was performed using additively manufactured thrusters constructed from Formlabs Clear Photopolymer Resin, Formulation FLGPCL02, for nozzle performance verification and thrust verification. The thrusters were designed by GreenScale Technologies and manufactured on site using a FormLabs 3D printer. Thrusters made from this material were used for low temperature and preliminary experimentation.

For thermal imaging of the plume and exit plane temperature measurement, a thruster was 3D printed by a third party using the DMLS process and a titanium alloy as the material of construction. The drawings for the titanium alloy thruster are shown in Figure 5.1, and the actual thruster used for testing is shown in Figure 5.2.

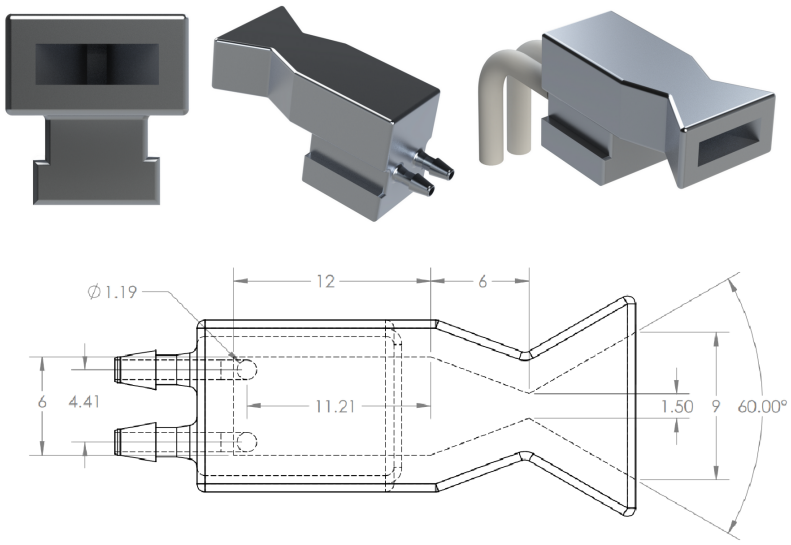

Figure 5.1: Drawings of additively manufactured thruster design used for experimental testing. Designed by GreenScale, LLC.

5.2 Nozzle Performance Verification

Schlieren photography was used to verify that the nozzle design can create supersonic flow at the nozzle outlet. In order to make this verification, compressed air at ambient temperature was supplied to the nozzle to mimic the flow of reaction products during thruster operation. Through this process, the plume created by the gasses at the outlet of the nozzle was observed using Schlieren photography. This allowed the flow to be visualized and analyzed for the expected supersonic flow patterns.

The converging-diverging nozzle can be approximated using isentropic quasi-one-dimensional flow. In order for the nozzle to produce a supersonic flow in the diverging section of the nozzle, the flow must have a pressure ratio over the nozzle which is equal to or exceeds the minimum pressure ratio necessary for sonic flow at the throat. This pressure ratio is dependent on the mixture of gases passing though the nozzle, and is

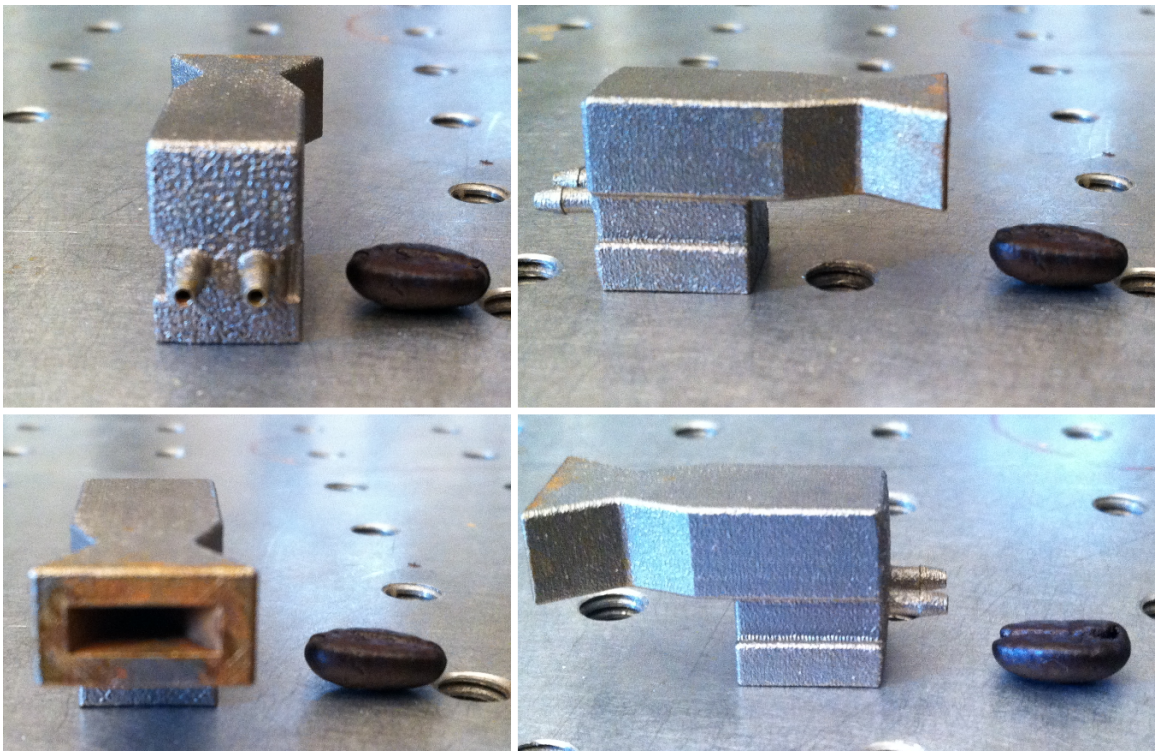

Figure 5.2: Additively manufactured thruster, manufactured with titanium alloy material. Thruster is shown side by side with a french roasted arabica coffee bean for scale. Photographs were taken after experimental testing, residual ferric chloride is seen as discolorations in the diverging section of the nozzle.

shown as Equation 5.1.

$$\frac{P^*}{P_0} = (\frac{2}{\gamma + 1})^{\frac{\gamma}{\gamma - 1}} \tag{5.1}$$

where $\frac{P^*}{P_0}$ is the minimum ratio of pressure upstream of the nozzle to the pressure on the nozzle exit plane in order to achieve sonic flow at the nozzle, and γ is the specific heat ratio of the gasses passing through the nozzle.

Due to the low Reynolds numbers in the nozzle, it was possible that the viscous effects in the nozzle could not be ignored and that Equation 5.1 would not accurately describe the nozzle. For supersonic viscous flow, viscous effects must be taken into

account when designing the nozzle because the subsonic boundary layers can occupy a large fraction of the divergent cross section resulting in a significant decrease in performance that is not accounted for in the isentropic quasi-one-dimensional model [71].

Schlieren photography was used to verify that the selected nozzle design will achieve supersonic flow in the divergent section. This is an important verification because it demonstrates that the nozzle will work as intended when implemented into the CubeSat propulsion system.

5.2.1 Background

Schlieren photography relies on the dependence of refractive index on gas density. It uses a collimated light source, a light source with parallel rays, which is focused with a mirror. A knife's edge is placed at the focal point of the mirror such to block approximately half of the light. Due to this, when the collimated light travels through a fluid of uniform density, the photograph appears darker than it would if some of the light was not blocked by the knife's edge. Through this process the image is not distorted in any way. However, when there are variations in density of the fluid which the collimated light travels through before being focused by the mirror, the refraction of the light caused by the changing refractive index of the fluid bends the ray of light. The rays that are no longer in line with the rest of the collimated light do not pass through the focal point of the mirror. Instead, they hit the knife's edge and are effectively removed from the photographed image.

Due to this, the light which passed through a fluid with varying density is blocked from the final image taken by the camera. The resulting photograph taken by a

Schlieren system contains the information from the collimated light, with lighter or darker areas which correspond to the density gradients in the fluid. This allows shock waves and shock patterns to be visualized as darker or lighter patterns in the Schlieren photograph [72, 73].

5.2.2 Method and Apparatus

The Schlieren photography was performed in house using ambient temperature compressed air through the nozzle. The house air stagnation pressure was measured to be approximately 55 $PSIg$. According to Equation 5.1, the ratio of the stagnation pressure to outlet pressure necessary to achieve sonic flow at the throat was 1.57 (using $\gamma = 1.4$ for air), resulting in a necessary minimum stagnation pressure of approximately 38 $PSIg$ when vented directly to the laboratory. Due to this, the pressure drop over the nozzle resulting from the supplied house air was determined to be theoretically large enough for supersonic flow in the divergent section of the nozzle.

The Schlieren photography apparatus is shown in Figure 5.3. The Schlieren apparatus used for this experiment was a Z-type system consists of a bright light source that passes through a 0.25 mm hole, directed at a mirror that is placed one focal length away from the light source. The first mirror collimates the light and redirects the collimated light over the test region, where the nozzle was placed. After passing through the test region, another mirror refocuses the light towards the knife's edge, in this case the edge of a razor blade, which is located one focal length from the second mirror. A camera after the knife's edge is used to capture the Schlieren photographs.

The 45 degree half angle nozzle design was chosen for Schlieren photography be-

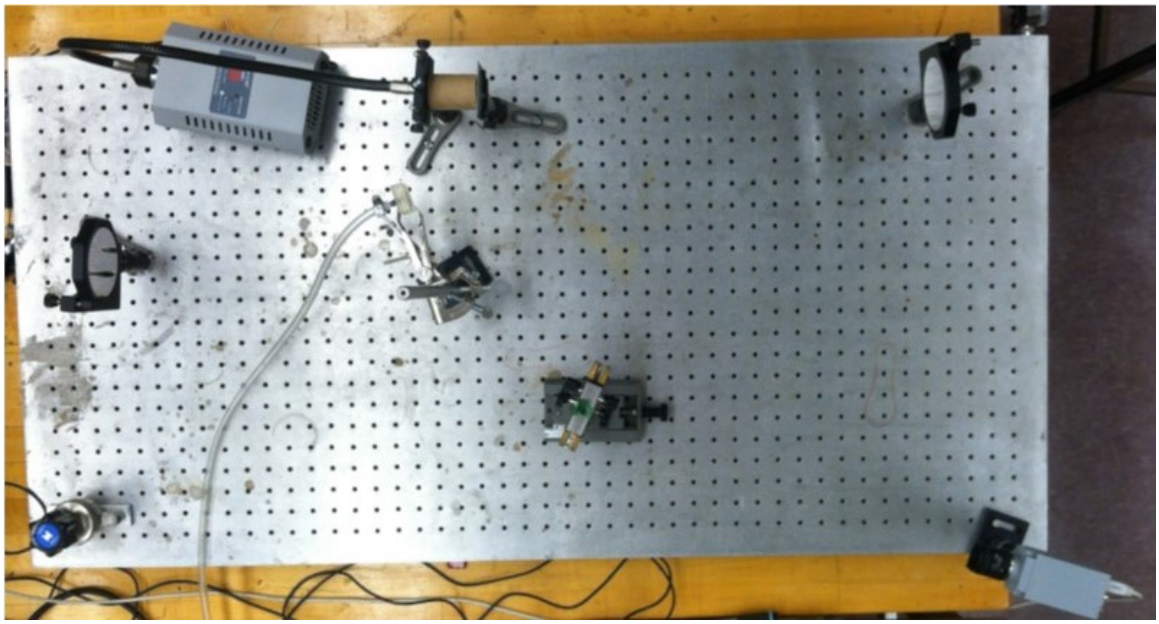

Figure 5.3: Optical table with the Z-type Schlieren photography system used for flow visualization of the nozzle plume. The light source is in the top left, and the camera is in the bottom right.

cause it had the highest predicted performance in numerical simulations. A simplified flow network design was created which eliminated one of the inlets from the nozzle design, leaving one inlet for the house air line. A photograph of the nozzle which was used for Schlieren photography is shown in Figure 5.4. The nozzle was additively manufactured using Formlabs Clear Photopolymer Resin, formulation FLGPCL02.

5.2.3 Results and Conclusions

The Schlieren photograph shown in Figure 5.5 shows an overexpanded diamond shock pattern in the flow exiting the nozzle. The presence of the standing shock structure is evidence of supersonic flow at the nozzle exit.

The results obtained from the Schlieren photography confirm that the nozzle op-

Figure 5.4: Nozzle with 45 degree half angle used for verification of supersonic flow in the test region of the in-house Schlieren photography system. The photo on the left shows the house air connection which was secured with epoxy, the photograph on the right shows the simplified flow network and nozzle half angle.

erates properly with stagnation pressures as low as 55 $PSIg$. Due to the rapid decomposition and combustion reaction during operation, it is likely that the chemical propulsion system will have adequate pressure upstream of the nozzle to achieve supersonic flow in the diverging section of the nozzle when operating in the vacuum of space.

5.3 Thrust Verification

After verification of supersonic flow in the divergent section of the 45 degree half angle nozzle, an effort was made to measure the thrust produced by the nozzle. Due to the large half angle of the nozzle, substantial geometric losses caused by the portion of the nozzle exit flow directed away from the axis of the nozzle were possible. Although the previously performed computational simulations suggest that

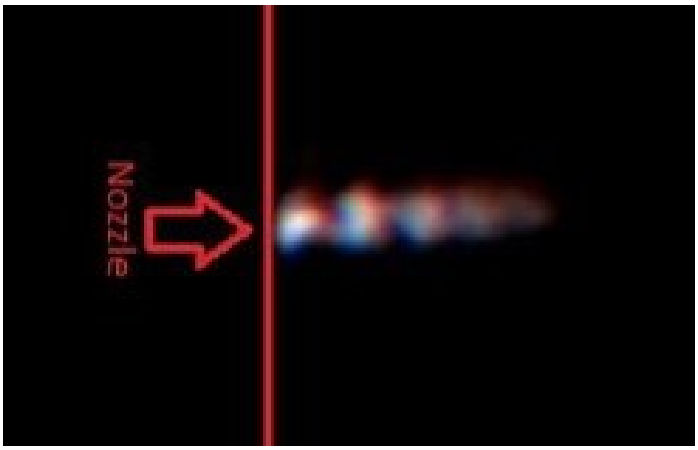

Figure 5.5: Schlieren photograph of ambient temperature air passing through the 45 degree half angle nozzle vented directly to the laboratory, with an upstream stagnation pressure of approximately 55 $PSIg$. An overexpanded diamond shock pattern is visible which is evidence of supersonic flow in the diverging section of the nozzle.

the use of a 45 degree half angle had improved performance over the 15 and 30 degree half angles, experimental thrust data is valuable for computational model validation. These experiments were performed in an effort to validate the computational model and determine if the thrust produced by the system would be adequate for the desired application.

5.3.1 Thrust Stand Background

A torsional thrust stand was constructed for steady state thrust measurements on the order of milli-newtons. This type of thrust stand was chosen for its simplicity and ease of use. A photograph of the thrust stand is shown in Figure 5.6.

The thrust stand operates through the deformation of a central spring. It was designed to have a sensitivity of 1.0 mN and a sampling rate of 20,000 $samples/second$. Position of the torsion arm is measured by a Lord MicroStrain Digital Voltage Re-

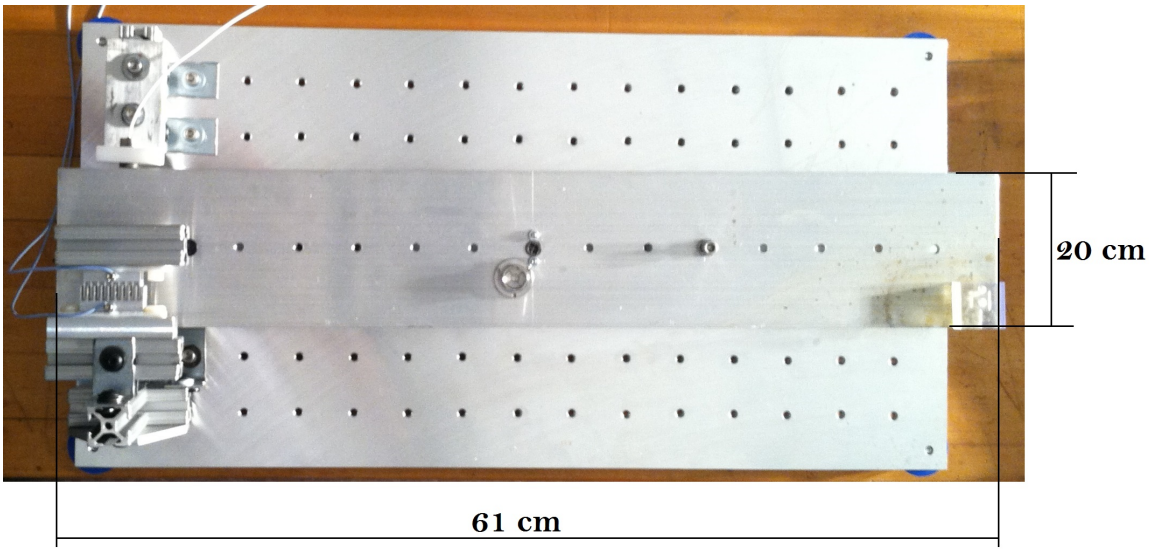

Figure 5.6: Photograph of the torsional thrust stand. A polymer nozzle is placed at the end of the thrust stand arm and the angular displacement of the arm is measured during thruster operation. The thrust produced by the nozzle is calculated from the arm displacement.

luctance Transmitter (DVRT), and captured using a National Instruments USB-6001 Digital Acquisition (DAQ).

A LabView Virtual Instrument was written to convert the positional data into thrust data, and record this data for post-processing. Hydrogen peroxide and catalyst solution are pumped into the thruster reaction chamber via two syringe pumps manufactured by New Era Pump Systems Inc., model NE-300.

5.3.2 Experimental Method

To perform thrust stand measurements, prototype thrusters were 3D printed using a FormLabs Form 1+ 3-D using FormLabs Clear V2 resin (FLGPCL02). The resin was chosen because it has been shown to be chemically inert when subjected to both hydrogen peroxide and the catalysts of interest. In addition to chemical compati-

bility, the Form 1+ is a Sterolithography (SLA) printer, which cures the resin using an ultraviolet laser. Due to this, the cured resin has a higher melting point when compared to the products of many other low cost additive manufacturing methods. High melting points are important because the material was subjected to the heat released from the decomposition of the hydrogen peroxide as well as the combustion of the catalyst solvent and must be capable of surviving the temperature of short duration firings without melting. Prototypes of the 45 degree half angle thrusters were manufactured in-house using the system described; an example of the thrusters used for thrust stand testing are shown in Figure 5.7.

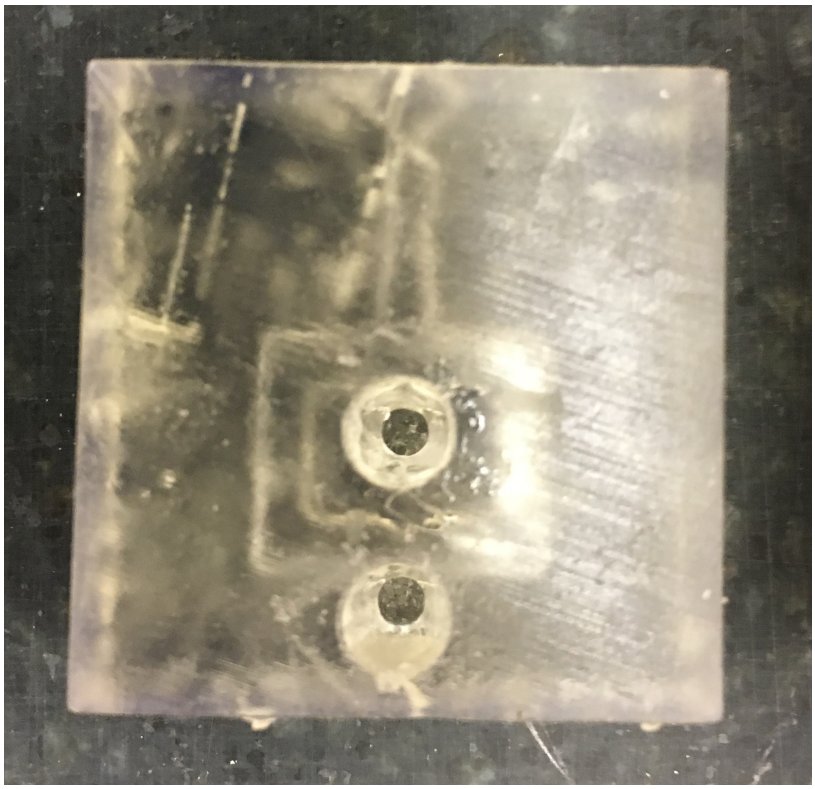

Figure 5.7: Photo of an additively manufactured thruster with a 45 degree half angle used for thrust stand testing. Catalyst solution was supplied to the top inlet port and hydrogen peroxide was supplied to the bottom inlet port.

The flow rates of the hydrogen peroxide and catalyst solutions into the thruster were controlled via syringe pumps attached to the thruster inlets using a lightweight, flexible, polymer tubing which offered negligible mechanical resistance against the movement of the thrust stand arm. The prototype thruster was then mounted to end of the thrust stand arm so the thrust vector was perpendicular to the arm. Data collection began once both the hydrogen peroxide and catalyst solutions entered the mixing chamber.

A photograph of a thruster during operation is shown in Figure 5.8.

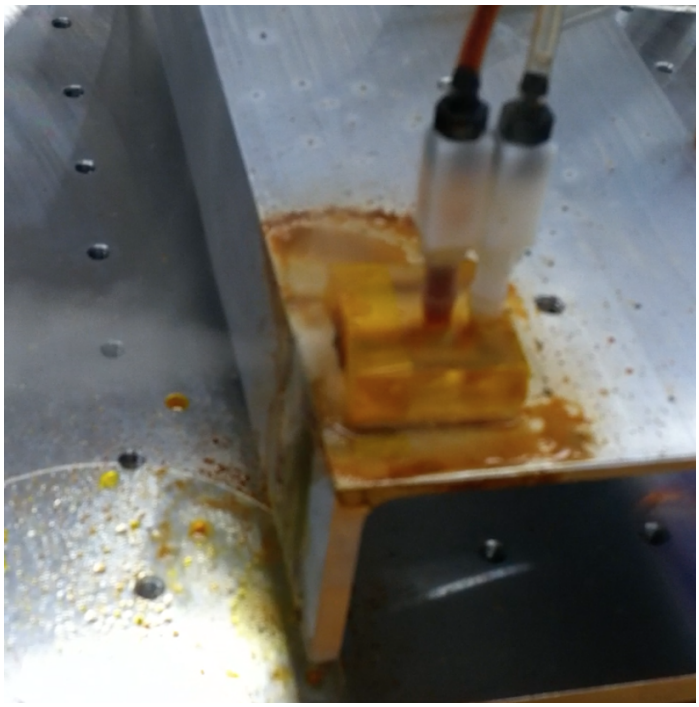

Figure 5.8: Photo of an additively manufactured thruster operating with hydrogen peroxide and 15% ferric chloride in 2-propanol.

Figure 5.8 shows a visible plume of condensed steam due to the ambient temperature in the laboratory, which is below the condensation point for water. The shape of the plume suggests that the thruster is operating as properly.

5.3.3 Preliminary Results

Experiments were performed on the thrust stand using a 45 degree half-angle prototype nozzle with a straight channel mixing and reaction chamber. For these experiments, 87.6% hydrogen peroxide was decomposed using water, ethanol, and 2-propanol as homogeneous catalyst solvents, ferric chloride was used as the catalyst. Based on the flow rates of hydrogen peroxide and catalyst solution, thrust levels between 20 mN and 70 mN were expected. Although the expected thrust lies in the measurable range of the thrust stand, no measurable thrust was produced during experimentation. As shown in Figure 5.8, the thruster operated as expected, but the thrust was likely below the threshold of the equipment.

Along with this, steady state operation of the thruster during preliminary testing was not achieved. This is because during extended periods of operation, the temperature inside the reaction chamber and the nozzle exceeded the maximum operating temperature of the Formlabs polymer material. The high temperatures resulted in the combustion of the polymer material before steady state data could be collected. A photograph of the charred thruster is shown as Figure 5.9

5.4 Thermal Imaging of Plume

5.4.1 Background

Thermal imaging was used to visualize the temperature profile inside the plume at the nozzle exit during operation. From the images captured during steady-state operation, the temperature of the plume and the temperature of the thruster was

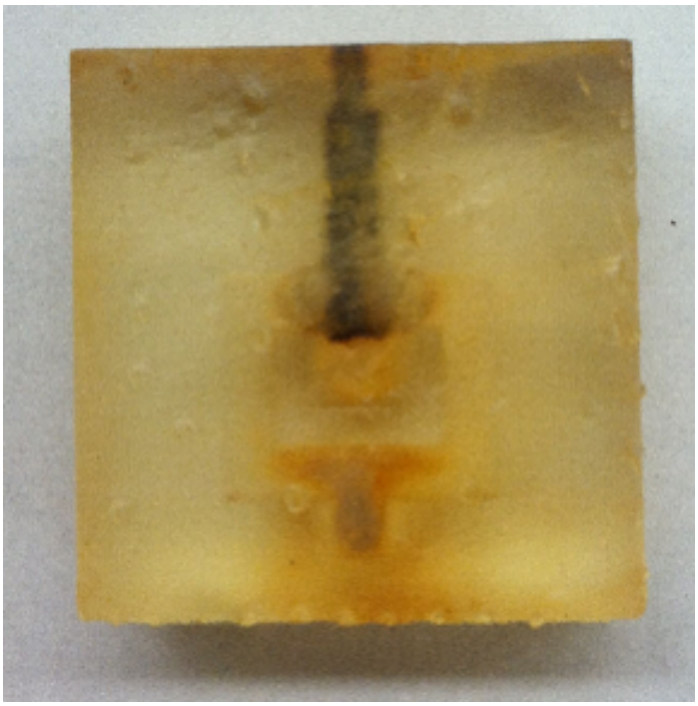

Figure 5.9: Photograph of a additively manufactured thruster operating with hydrogen peroxide and 15% ferric chloride in 2-propanol.

observed and compared. The thermal image of the plume was used to determine the shape, direction, and temperature characteristics of the flow after exiting the nozzle. From these data, the ratio of catalyst solvent to hydrogen peroxide as well as the total flow rate of gases through the nozzle were examined to determine which parameters affect the operation of the propulsion system.

During operation in the supersonic regime, temperature of the working fluid after exiting the nozzle is significantly lower than the temperature upstream of the nozzle. Because the reaction chamber is inside the thruster, directly upstream of the nozzle, the plume temperature was expected to be much lower than the temperature of the thruster during steady-state, supersonic operation. Although the thermal camera was not calibrated to measure absolute temperatures of the materials, the thermal images

provide invaluable insight in the flow dynamics and operation of the system.

5.4.2 Experimental Procedure

Thermal imaging of the system was performed using a thermoIMAGER TIM T900 manufactured by Micro-Epsilon. Thermal images were collected and analyzed using Micro-Epsilon's thermal imaging software, TIM Connect. Along with thermal images, standard video was recorded using a PixeLink PL-B774U Color Camera. The thermal imaging camera was supported above the thruster, while the PixeLink camera was mounted to capture the side view of the thruster.

Two New Era Pump Systems, Model No. NE-300, syringe pumps were used to supply aqueous catalyst solution and hydrogen peroxide to the thruster. A photograph of the experimental set-up is shown below in Figure 5.10.

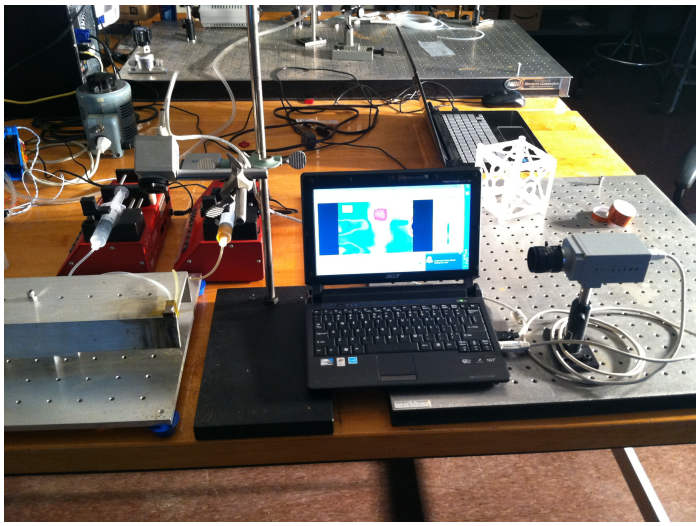

Figure 5.10: Photograph of thermal imaging set-up including thermal imaging camera, PixeLink camera, syringe pumps, and DMLS thruster.

The thruster used for this experiment was manufactured from a titanium alloy

through the DMLS process. The thruster had a 1.5 mm throat, a throat to exit area ratio of 6, and a linear geometry. The thruster used for this experiment is described in Section 5.1.

To remain below the melting point of the nozzle, water was used as the catalyst solvent which decreased the adiabatic flame temperature well below the melting point of the titanium alloy. The use of water as the solvent eliminated the combustion of the catalyst solvent. This, along with the control of the ratio of hydrogen peroxide to aqueous catalyst solution allowed the expected adiabatic flame temperature during steady-state operation to be set less than 685 Kelvin for each trial. The low adiabatic flame temperature insured that the thruster would be available for future testing.

The catalyst solution used for experimentation was 15 weight% aqueous ferric chloride. The ferric chloride was laboratory grade, anhydrous powder, manufactured by The Science Company. Catalyst solution was prepared less than an hour prior to testing in order to eliminate any possible catalyst degradation due to oxygen exposure. Hydrogen peroxide used for the experiment was HTP manufactured by FMC Corporation, the concentration was measured as 87.6 % using an Atago refractometer, model PAL-39S.

5.4.3 Experimental Results

The thermal image data shows that during operation the plume was a lower temperature than the thruster. This is shown in Figure 5.11, where the plume is blue, the surrounding laboratory atmosphere is green, and the thruster is yellow. During steady-state operation, the temperature of the thruster was closely related the stagnation temperature of the fluid upstream of the nozzle throat. These results show

that there was a significant decrease in temperature as the fluid passed through the nozzle. This strongly suggests that the nozzle was operating in the supersonic flow regime.

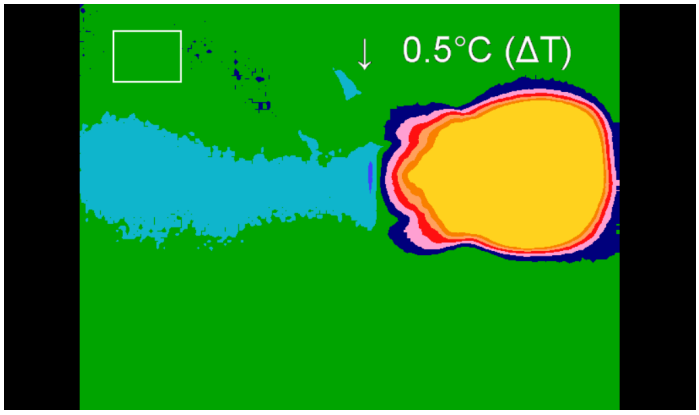

Figure 5.11: A thermal image of steady-state operation of the thruster using 15% aqueous ferric chloride as the catalyst solution and 87.6% HTP. The large temperature difference between the thruster and plume suggests supersonic operation.

Figure 5.12 shows the plume created by the nozzle during steady-state operation. At low total gas flow rates, the plume was stable during operation.

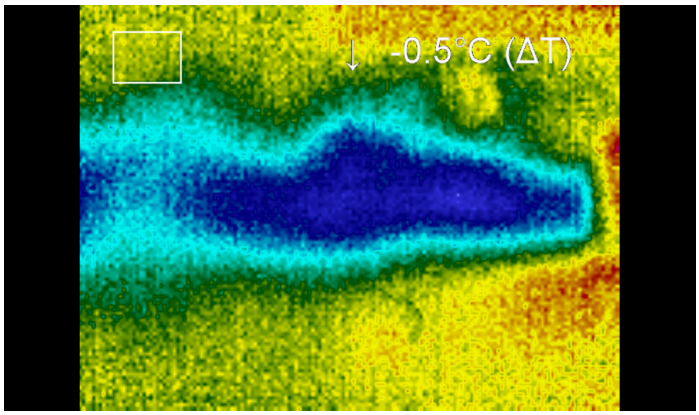

Figure 5.12: A stable plume created by the thruster at low gas flow rates.

At high gas flow rates, the plume developed instabilities which caused the direction of the plume to bounce between the walls and the center of the nozzle. When the

flow direction changed, no noticeable changes in plume temperature or flow patterns were observed suggesting that the nozzle was operating in the supersonic flow regime regardless of the flow instabilities. The instabilities in the flow direction were likely caused by incomplete mixing resulting in incomplete reaction in the thruster reaction chamber. This would cause suspended liquid droplets in the working fluid during high operational flow rates. The observed flow instability can be seen in Figure 5.13.

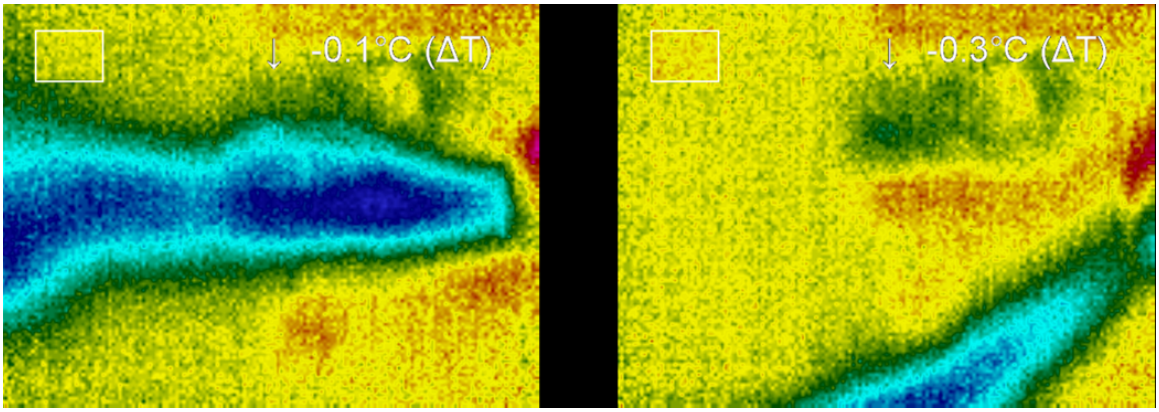

Figure 5.13: A flow instability at high flow rates through the thruster system. These instabilities are likely caused by incomplete mixing and reaction upstream of the nozzle.

5.5 Exit Plane Temperature Measurement

5.5.1 Background

The temperature of the working fluid at the exit plane of the nozzle indicates if the flow through the nozzle is in the supersonic regime. Supersonic flow through the nozzle is achieved if the pressure drop over the nozzle is high enough to choke the

flow at the nozzle throat. As the nozzle diverges, a supersonic flow will accelerate as the flow area increases. The flow through a converging-diverging nozzle can be described using the quasi-one-dimensional isentropic relation shown as Equation 5.2. Equation 5.2 relates the Mach number, M, the ratio of the flow area to the area of the throat, $\frac{A}{A^*}$, and the specific heat ratio of the gasses flowing through the nozzle, γ.

$$\left(\frac{A}{A^*}\right)^2 = \frac{1}{M^2}\left[\frac{2}{\gamma+1}\left(1+\frac{\gamma-1}{2}M^2\right)\right]^{\frac{\gamma+1}{\gamma-1}} \tag{5.2}$$

From this relationship, the geometry of the nozzle can be used to determine a theoretical Mach number at the nozzle exit plane. Using the temperature relation for isentropic supersonic flow, shown as Equation 5.3, this information can then be used to determine the ratio of the stagnation temperature, T_o, to the temperature at the nozzle exit plane, T_e, where M_e is the Mach number at the exit plane.

$$\frac{T_e}{T_o} = \left(1+\frac{\gamma-1}{2}{M_e}^2\right)^{-1} \tag{5.3}$$

The adiabatic flame temperature of the reactants for each trial is the approximate stagnation temperature in the system. From this, it is possible to determine a theoretical working fluid temperature at the exit plane of the nozzle. These calculations result in the lowest achievable fluid temperature at the exit plane during experimentation due to the isentropic assumptions made in the calculation of the fluid exit temperature.

These calculations allow the experimental exit plane temperature to be compared to the theoretical temperature which would be achieved if the nozzle was operating in the supersonic regime at isentropic conditions.

5.5.2 Experimental Procedure

The exit plane temperature measurement was performed using an Omega digital thermometer, model HH501AK, and a type K thermocouple. The thermocouple was placed directly at exit plane of the nozzle so that the end of the thermocouple was in the center of nozzle exit. A thermal camera manufactured by Micro-Epsilon, model TIM T900, was also used to capture thermal images of the plume during the tests. Along with thermal images, standard video was recorded using a PixeLink PL-B774U Color Camera. The experimental set-up for this experiment was similar to the experimental set-up for the thermal imaging of the plume experiment. The experimental set-up for this experiment is shown in 5.14.

Figure 5.14: Right: Photograph of DMLS titanium nozzle used for plume temperature measurement. A type K thermocouple was placed directly in the center of the nozzle exit for temperature measurements. Left: Photograph of entire experimental set-up including thermal imaging camera, video camera, and digital thermometer.

Figure 5.15 shows a photograph of the thruster during the plume temperature measurement experiment. In this photograph, the thermocouple placement in the

center of the nozzle exit can be seen. Condensation of steam produced by the reaction is visible around the nozzle exit plume. From the experimental data, thermal images, and photographs, the thruster appeared to be operating normally, with the exception of flow instabilities at high flow rates, during all trials.

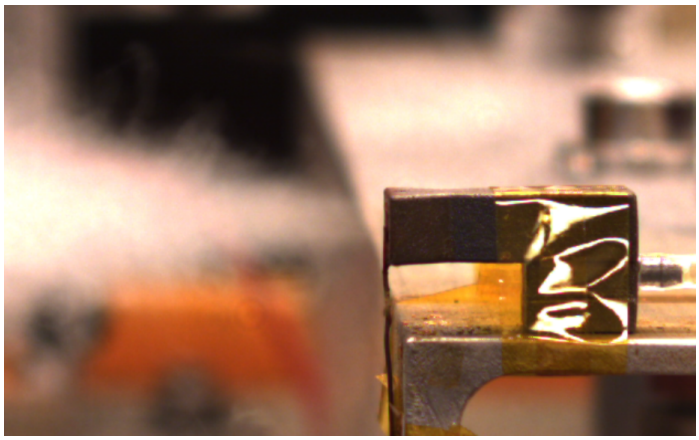

Figure 5.15: A photograph of the thruster system operating during the plume temperature measurment experiment. Condensation surrounding the plume is visible.

To remain below the melting point of the titanium alloy used for the nozzle fabrication, water was used as the catalyst solvent. This eliminated the combustion of the catalyst solvent resulting in manageable adiabatic flame temperatures. By controlling the ratio of hydrogen peroxide to aqueous catalyst solution, the maximum adiabatic flame temperature expected during steady-state operation of the thruster was 685 Kelvin.

The catalyst solution used for experimentation was 15 weight% aqueous ferric chloride. The ferric chloride was laboratory grade, anhydrous powder, manufactured by The Science Company. Catalyst solution was prepared less than an hour prior to testing in order to eliminate any possible catalyst degradation due to oxygen exposure. Hydrogen peroxide use for the experiment was HTP manufactured by FMC

Corporation, the concentration was measured as 87.6 % using an Atago refractometer, model PAL-39S.

5.5.3 Experimental Results

From Equations 5.2 and 5.3, the measured temperatures were normalized by the theoretical supersonic isentropic fluid temperature at the exit plane. The resulting ratio is plotted against the ratio of the flow rate of HTP to catalyst solution for each run in Figure 5.16. This plot shows that the measured temperatures of the working fluid at the nozzle exit agree within 18% of the calculated theoretical isentropic temperature when a volumetric ratio of 10 units HTP to 1 unit of catalyst was used. The closest measured temperature at this ratio agreed within 3.5% of the theoretical value. Along with the strong agreement with theoretical values at high volumetric ratios of HTP to catalyst solution, it is noteworthy that none of the recorded temperatures were below the minimum isentropic values.

Due to the strong agreement between the calculated quasi-one-dimensional isentropic and measured exit plane temperatures, this nozzle and mixing scheme were likely operating as expected during steady-state operation. These data also suggest, that at the nozzle scale which was tested, the viscous boundary layers do not significantly decrease the exit area of the nozzle as was predicted by Louisos in supersonic micronozzles [67].

Figure 5.17 compares the measured temperatures to the adiabatic flame temperature. This shows that low ratios of HTP to catalyst solution resulted in measured nozzle exit plane temperatures near the adiabatic flame temperature. This trend is observed in flows with volumetric ratios 4, 2, and 1. These data suggest that flows

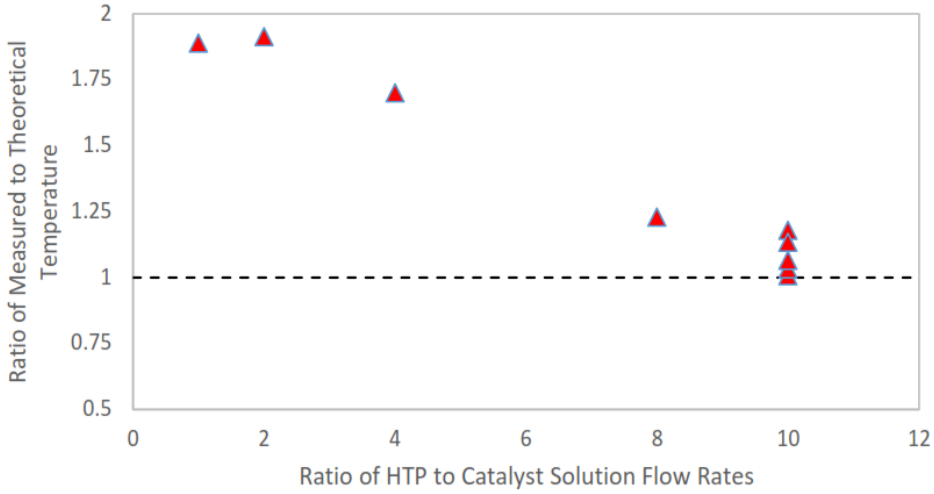

Figure 5.16: The ratio of measured to theoretical temperature vs. the ratio of volumetric flow rate of HTP to catalyst solution. High ratios of HTP to catalyst solution show agreement with quasi-one-dimensional isentropic supersonic flow in the nozzle. This strongly suggests the flow through the nozzle is choked at the throat at high HTP to catalyst solution ratios.

with low ratio of HTP to catalyst solution were not able to generate enough energy to create sufficient stagnation pressure to achieve choked flow at the throat. Due to this, these flows remained in the subsonic regime in the nozzle, resulting in much higher nozzle exit plane temperatures.

During experimentation, the total molar flow rate of gases through the nozzle varied between trials. The ratio of the measured nozzle exit plane temperature to theoretical quasi-one-dimensional isentropic temperature is shown as a function of total molar gas flow rate in Figure 5.18. This plot shows that the total gas flow rate had little affect on the resulting flow regime. This plot strongly suggests that high ratios of HTP to catalyst solution result in supersonic flow though the nozzle, even at low total gas flow rates.

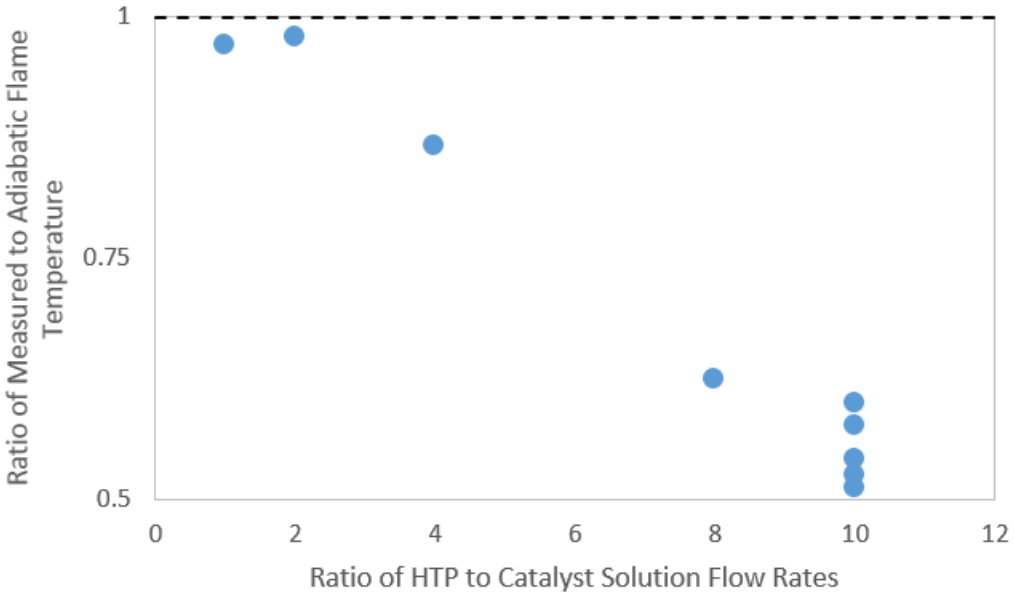

Figure 5.17: The ratio of measured to adiabatic flame temperature vs. the ratio of volumetric flow rate of HTP to catalyst solution. These data strongly suggest that at low ratios of HTP to catalyst solution, flow is not choked at the nozzle throat and remains in the subsonic regime throughout the nozzle.

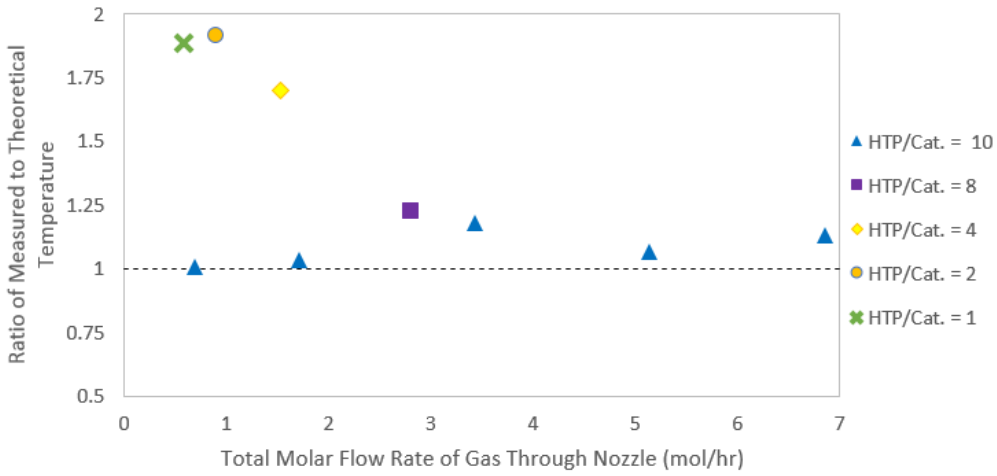

Figure 5.18: The ratio of the measured to theoretical temperature plotted against the total molar flow rate of gas through the nozzle. High ratios of HTP to catalyst solution show evidence of supersonic flow over the entire range of flow rates.

Chapter 6

Future work

6.1 Thermal Management

During steady-state operation, the high adiabatic flame temperatures achieved through the decomposition of hydrogen peroxide and combustion of catalyst solvent causes the temperature of the mixing and reaction chamber and nozzle to be greater than the melting point of the material of construction. Although the thermal mass of the material of construction may have the ability to absorb the heat for short firings, extended use of the thrusters for bipropellant operation causes concern. The current configuration, without an additional cooling scheme, may result in melting, deformation, and ultimately failure of the propulsion system during steady-state operation.

Due to this, the addition of a cooling system will allow the thruster to operate in steady-state bipropellant mode by lowering the operating temperature of the material and eliminating concerns of overheating. Through the use of cold liquid reactant, a preheater will be designed which will transfer heat produced from the reaction into the reactants before they are fed into the mixing chamber, keeping the reaction chamber

and nozzle temperatures low enough for continuous operation. This type of nozzle and reaction chamber cooling scheme is typical of chemical propulsion systems and has proven to be effective cooling method in many aeronautical applications.

6.2 Mixing and Reaction Chamber Design

Thermal imaging of the plume showed flow instabilities which were likely caused by incomplete reaction in the thruster's mixing and reaction chamber. Incomplete reaction results in suspended liquid droplets in the flow, causing flow instabilities and potentially to decreasing thrust [60]. Instabilities were observed at high total gas flow rates suggesting that the hydrogen peroxide and catalyst solution were unable to mix and react completely before being ejected through the nozzle.

For these experiments, a straight channel geomerty was used for mixing of the hydrogen peroxide and catalyst solutions. Through the lengthening of the mixing and reaction chamber, it may be possible to achieve complete decomposition for high flow rate operation. A simple solution to this problem may be matching the residence time in the mixing chamber during high flow rate operation with the residence time of the stable, lower flow rate operation. Another solution may be to alter the mixing scheme from a straight channel to a more complex geometry. To date, many effective mixing schemes have been created for small scale, low Reynolds number flows which work through the generation of laminar chaos in the flow. These designs are often simple and include obliquely oriented grooves on one chamber wall, asymmetric herringbone patterns, or helical channels [74, 75].

6.3 Reliability Studies

Preliminary results show catalyst deposits on the nozzle walls. This deposition occurs when the liquid catalyst solvent reacts with hydrogen peroxide to form gaseous products. As the reaction proceeds, the volume of the catalyst solvent decreases leading to an increased catalyst concentration. When the solubility limit of the mixture is exceeded, the solid catalyst begins to precipitate out of solution. Eventually, all of the liquid reactants have formed gaseous products and the solid catalyst cannot remain in solution.

During operation, the catalyst particles are either entrained in the gaseous product stream and ejected through the nozzle or deposited as crystal structures on the walls of the reaction chamber and nozzle. In order to reduce the build up of catalyst deposits, it may be beneficial to manufacture the mixing chamber and nozzle with a resistant material or coating. However, since no long term operational studies have been performed on the nozzle, it is not clear if deposit build up occurs to a high enough degree to affect performance over the lifetime of the system. Through performing long term steady-state and pulsed mode operational testing, the accumulation of catalyst in the reaction chamber and nozzle during a normal operational lifetime can be quantified. From these results, it will be possible to determine if catalyst accumulation is a problem and if so, a method for resolving the issue can be developed.

Chapter 7

Conclusions

The CubeSat chemical propulsion system described in this paper utilizes a homogeneous catalysis gas generation scheme to provide bipropellant and pseudo-monopropellant operation modes. Dual mode operation is controlled by adjusting the ratios of catalyst solution to hydrogen peroxide fed to the thrusters. Pseudo-monopropellant mode occurs at the smallest possible ratio of catalyst solution to hydrogen peroxide. At this ratio, the thrust and impulse bit produced by the system approaches the performance of monopropellant hydrogen peroxide. Increasing the ratio of catalyst solution to hydrogen peroxide to the stoichiometric ratio allows the thruster system to operate in bipropellant mode. In this mode, the catalyst solvent is combusted using the hydrogen peroxide as an oxidizer. This greatly increases the thrust, impulse bit, and specific impulse provided by the system. Dual mode operation allows the same propulsion system to be used for small position adjustments such as attitude control as well as more demanding maneuvers such as rapidly traversing the Van Allen belts.

The nozzles, mixing and reaction chamber, piping, manifolding, and chemical storage, can be additively manufactured directly into the CubeSat chassis without

violating CubeSat regulations. Commercial off the shelf parts can be used for the valving, the only component of the system which cannot be additively manufactured. The incorporation of the propulsion system into the chassis allows for a low cost and highly customizable propulsion system which occupies a small fraction of the internal CubeSat volume. Additionally, the propellants used in the homogeneous catalysis scheme are non-toxic, "green" chemicals with a history of safe industrial usage.

This system provides a novel solution for low cost CubeSat propulsion. By leveraging microscale effects, the total mass and volume of this system is less than the alternative commercially available CubeSat propulsion systems. Through the work presented herein, three major goals were accomplished:

1. A "green" catalyst solution was selected for operation of the homogeneous catalysis system

2. The operation of the homogeneous catalysis system was experimentally validated as a viable gas generation method for CubeSat propulsion

3. Supersonic flow was validated using the selected nozzle design with cold compressed house air as well as with hot gas generated via the prototype homogeneous catalysis gas generation scheme

The achievement of these goals strongly supports the further development of the additively manufactured, homogeneously catalyzed, "green" chemical propulsion system described in this paper.

7.1 Catalyst and Catalyst Solvent Selection

15 weight % ferric chloride in 2-propanol was chosen as a high performing catalyst solution. 2-propanol was selected based primarily on its high energy density, high relative specific impulse, and fast reaction kinetics. Ferric chloride was selected as the catalyst due to its ability to dissolve in 2-propanol, ease of handling, high performance, and long term reliability. The 15 weight % solution of ferric chloride in 2-propanol performed well in both the solubility and drop testing experiments. Along with this, ferric chloride and 2-propanol are both "green" chemicals which are easily handled and have proven their safety through decades of use in industry. This catalyst solution is expected to allow for high performance operation in both pseudo-monopropellant and bipropellant operation modes of the homogeneous catalysis system.

7.2 Homogeneous Catalysis Validation

Through thermal imaging of the plume and exit plane temperature measurement experiments, the homogeneous catalysis gas generation system has been validated. The homogeneous method of gas generation proposed in this work successfully creates adequate pressure and flow rate in the mixing and reaction chamber to support steady-state, supersonic operation of the converging-diverging nozzle. Although these experiments showed signs of flow instabilities at high gas flow rates which were attributed to incomplete reaction in the mixing and reaction chamber, low gas flow rates

operated as expected. It is likely that these instabilities will be eliminated through the increase of residence time and the implementation of a passive mixing scheme in the mixing and reaction chamber.

7.3 Supersonic Flow Validation

Thruster nozzle design was based on the work of Louisos [67], utilizing a linear walled design to enhance performance on the small scale. The nozzle design was validated though Schlieren photography using house air as a working fluid. The resulting Schlieren photographs showed an overexpanded diamond shock pattern at the nozzle exit, confirming supersonic operation of the nozzle. Additionally, supersonic flow through a similarly designed, additively manufactured (DMLS), titanium alloy nozzle was confirmed using nozzle exit plane temperature measurements during hot gas operation. The hot gas was generated from the homogeneous catalysis gas generation scheme using 87.6 % hydrogen peroxide and 15 weight % aqueous ferric chloride as propellants. Thermal images and photographs were taken during operation of the prototype system. These thermal images show that the system operated as expected when the reacting flow had adequate mixing and residence time to completely react before entering the nozzle. Through these experiments, successful operation of the system was validated.

Appendix A

Propulsion System Drawings

This section includes preliminary drawings of a primary propulsion system and reaction control system that have been designed around the homogeneous catalysis scheme being studied. Figures A.1 and A.2 show the primary propulsion design, Figures A.3 and A.4 show the reaction control system design. These designs were drafted by GreenScale Technologies, LLC.

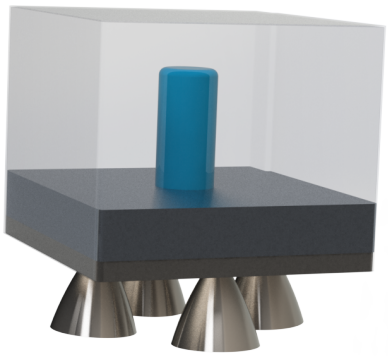

Figure A.1: Three dimensional drawing of the primary propulsion system not incorporated into the CubeSat chassis. The primary propulsion system is designed to consume 1 U of a CubeSat.

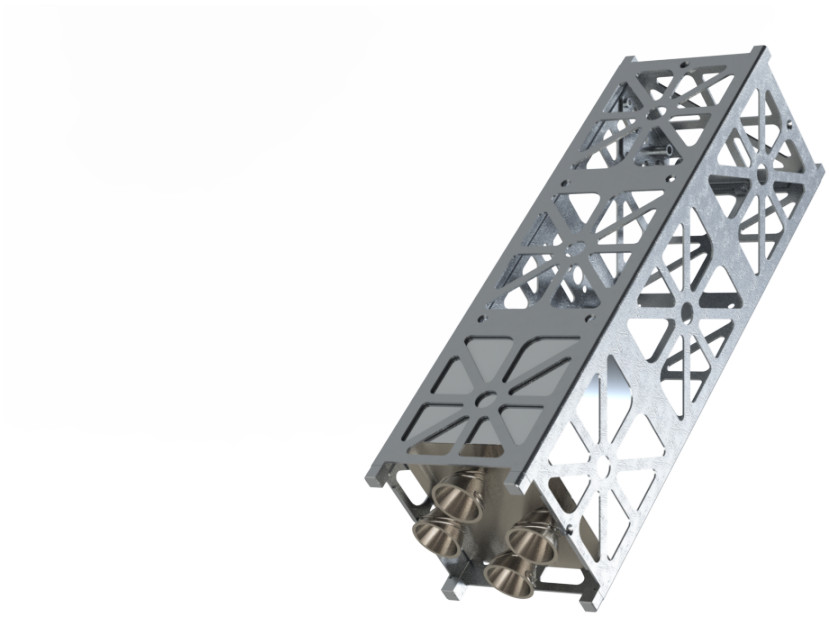

Figure A.2: Three dimensional drawing of the primary propulsion system incorporated into a 3 U CubeSat chassis.

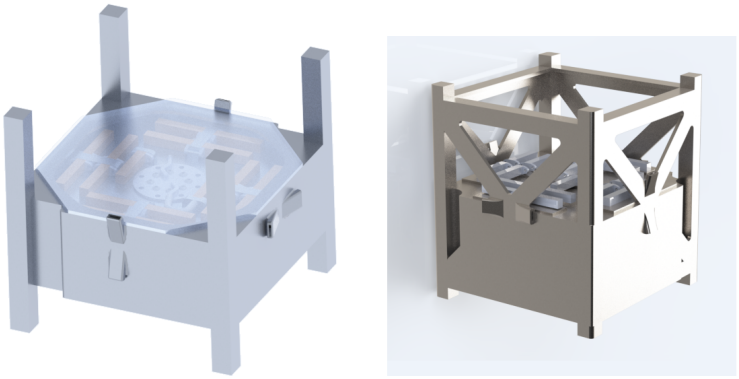

Figure A.3: Three dimensional drawing of the reaction control system (RCS) unit, not incorporated into a CubeSat. The RCS is designed to consume 1 U of a CubeSat.

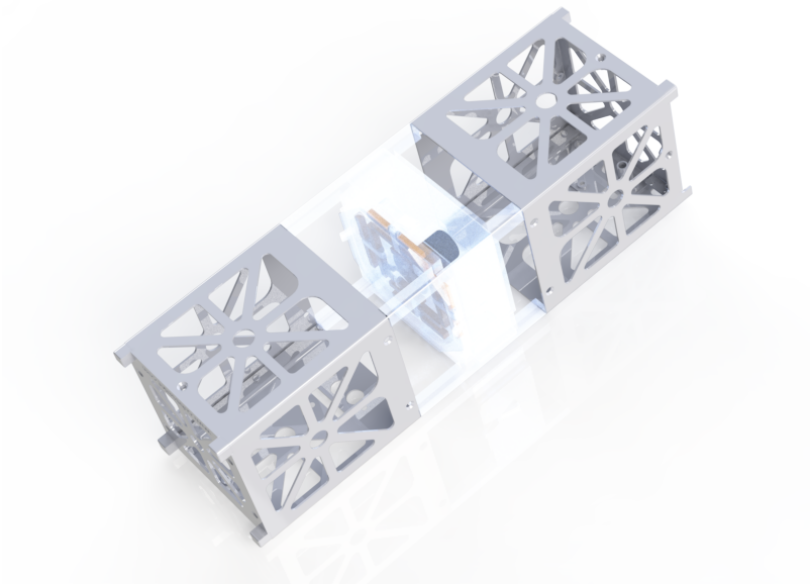

Figure A.4: Three dimensional drawing of the reaction control system (RCS) incorporated in the CubeSat chassis. The RCS is designed to consume 1 U of a CubeSat.

Appendix B

Nozzle Computational Model

For ease-of-manufacturability, the nozzle for this design is a linear micronozzle. Three-dimensional models have been developed for expander half angles of 15°, 30° and 45° with nozzle depths of 0.25 mm, 0.50 mm and 1.0 mm; all other geometric parameters are held constant. An example of the computational domain is shown in Figure B.1. The throat and exit dimensions of the micronozzle (0.5 mm and 3.0 mm, respectively) yield an expansion ratio of 6.0 and are fixed parameters in this study. To maintain a constant area expansion ratio, the axial length of the expander section is adjusted accordingly. The inlet stagnation temperature is held constant at 886 K, which is the adiabatic flame temperature of 85% hydrogen peroxide, while the inlet stagnation pressure is adjusted from 5 - 250 kPa, which corresponds to a Reynolds number of approximately 15 to 800.

Computational meshes are generated in COMSOL Multiphysics 5.1; a mesh sensitivity study was performed to confirm that simulations are insensitive to further refinements in the grid. The resulting meshes are between 200,000 and 300,000 elements depending on the expander angle and depth. Planar symmetry is used to

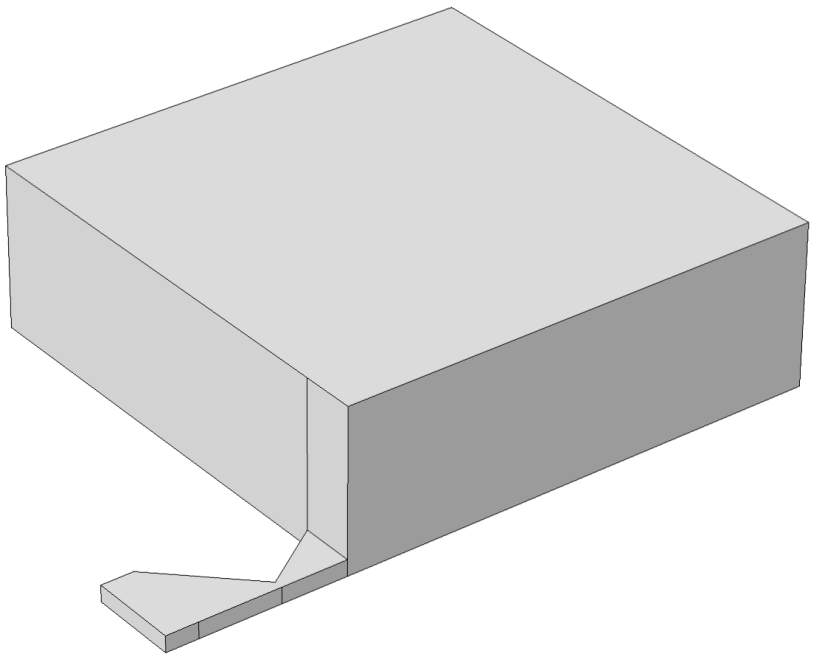

Figure B.1: Example of the computational domain for the numerical studies. The nozzle and an exit volume are modeled using planar symmetry to reduce the size of the domain.

reduce the computational domain. An example of the computational grid is shown in Figure B.2.

For each of the half angles and nozzle depths, a parametric sweep was run for six Reynolds numbers ranging between 50 and 800, for a total of 54 simulations. The stagnation pressure is ramped from 0 to the desired value over a period of 10 ms for stability, but for the purposes of this effort, transient effects are not considered. The thrust produced by each nozzle was evaluated according to Equation B.1.

$$\vec{F_t} = \int_{A_{exit}} \rho\vec{u}(\vec{u}\cdot\vec{n})dA + \int_{A_{exit}} (p_{exit} - p_\infty)dA \tag{B.1}$$

where $\vec{F_t}$ is the thrust, ρ is the density of the products at the nozzle exit plane, $\vec{u}$ is the velocity of the products at the exit plane, $\vec{n}$ is normal vector of the exit plane,

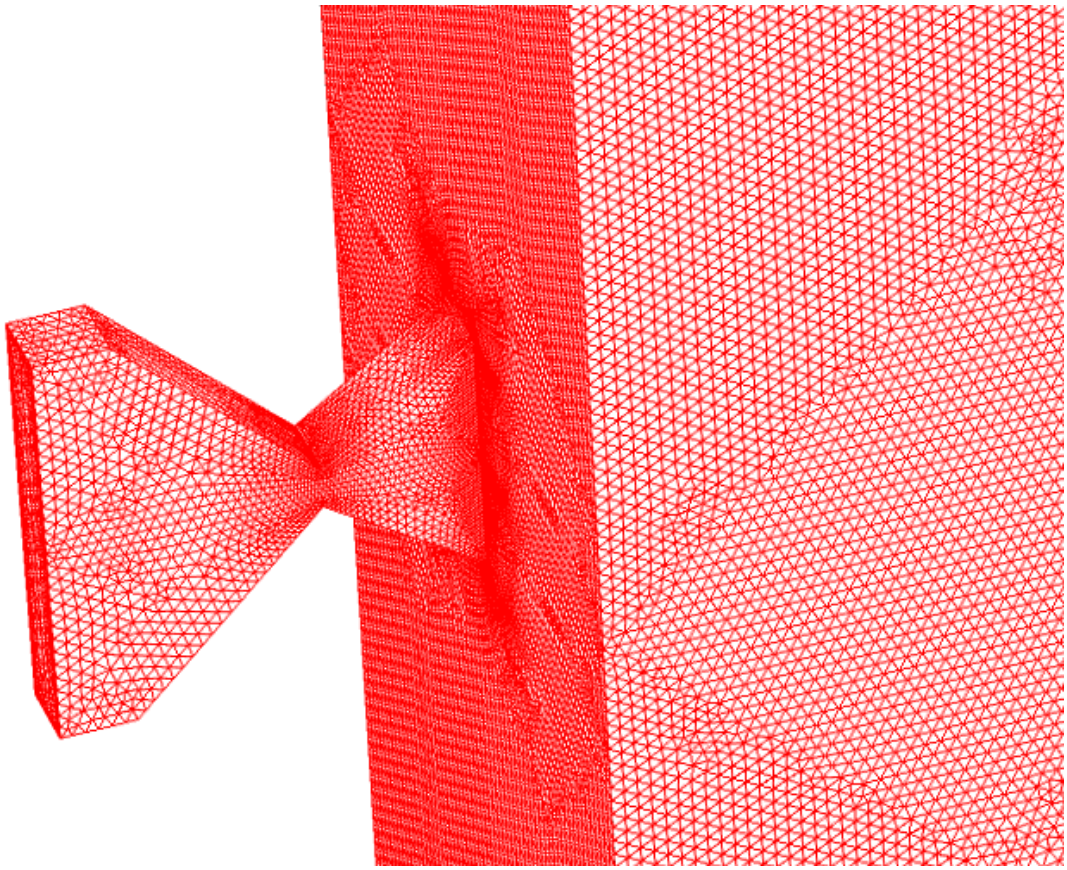

Figure B.2: Example of the computational mesh for a 30° half angle nozzle at 1 mm depth.

p_{exit} is the pressure at the exit plane and p_∞ is the ambient backpressure. In practice, for the micronozzles studied here, the pressure term contributes a negligible amount of thrust.

B.1 Nozzle Numerical Results

To orient the reader, an illustration of the 3D supersonic Mach contours in a 1 *mm* deep micronozzle is provided in Figure B.3 for a 30° expander half-angle operating at a throat Re 800. The supersonic Mach contours range from 1.0 to 3.25 and show

the expansion fan that is typical of an under-expanded nozzle.

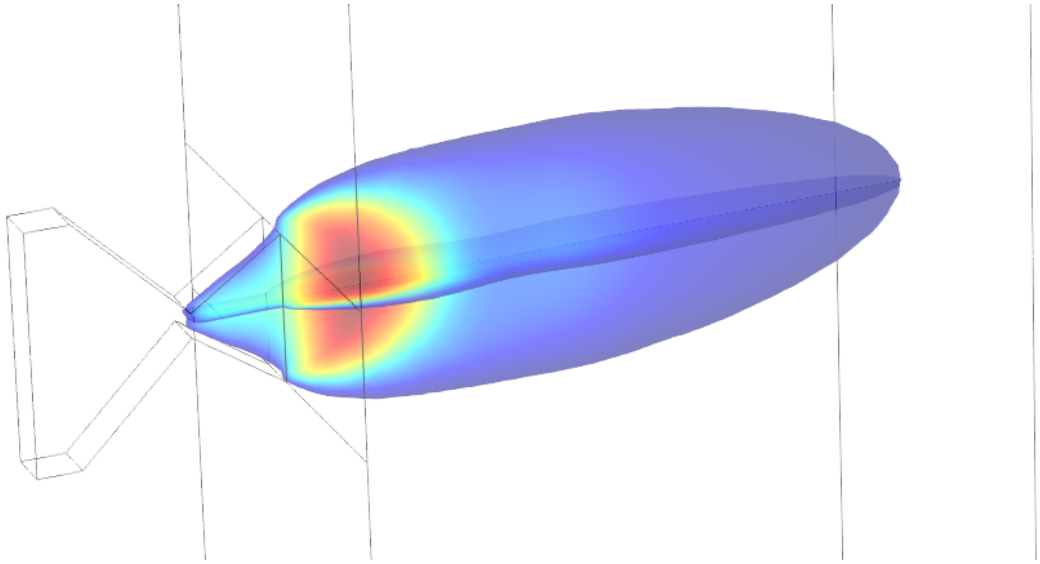

Figure B.3: The 3D supersonic Mach contours along the symmetry planes for a 1 mm deep micronozzle with a 30° expander operating at a throat Re ≈ 800.

An important consideration in micronozzles are the size of the subsonic region that develops as a result of the viscous boundary layer. While the subsonic region may be negligible for larger nozzles, it can become a significant percentage of the total nozzle exit for smaller nozzles. An illustration of the subsonic region for the same nozzle (1 mm depth, 30° half angle, Re ≈ 800) is shown in Figure B.4. Under these operating conditions, the subsonic layer is relatively small.

One of the major considerations of the numerical study is for nozzle depth. For the shallowest depth considered (0.25 mm), viscous forces are dominant owing to the subsonic layer; the boundary layers from the top and bottom of the nozzle are so large that for nearly all Reynolds numbers the flow is subsonic. The 45° expander has the smallest subsonic layer for all nozzle depths considered while the 15° has the largest subsonic layer size. The thrust produced per unit depth, shown in Figure B.5, shows

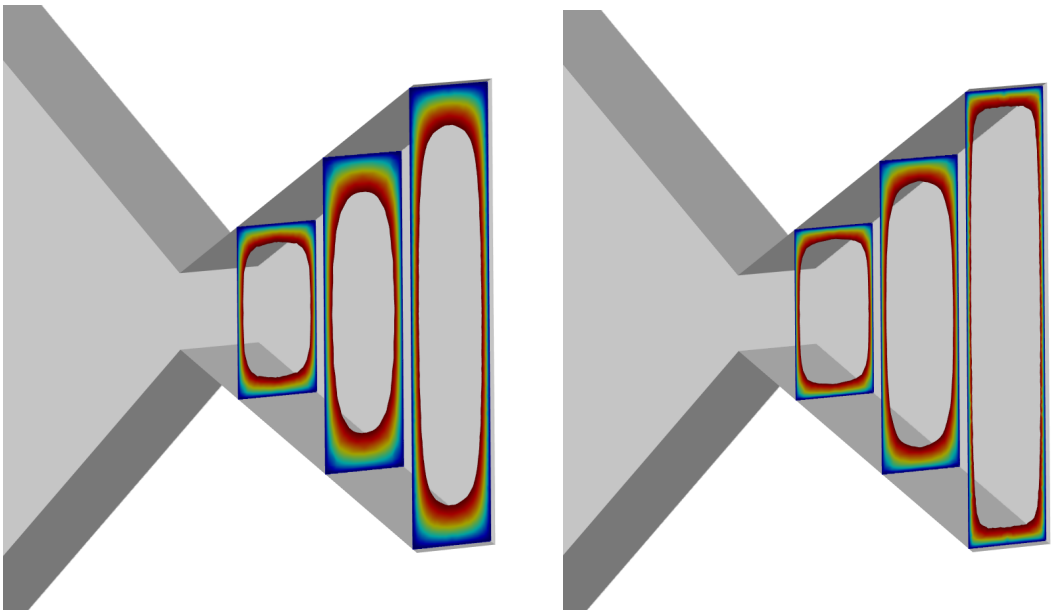

Figure B.4: An illustration of the 3D subsonic layers at selected locations in a 1 mm deep 30° expander operating at Re ≈ 200 (left) and 800 (right). Note the central core of the flow remains supersonic downstream of the nozzle throat in both, but the subsonic layers are noticeably larger for the lower Re.

that for the conditions simulated the 45° expander offers the best performance at all depths.

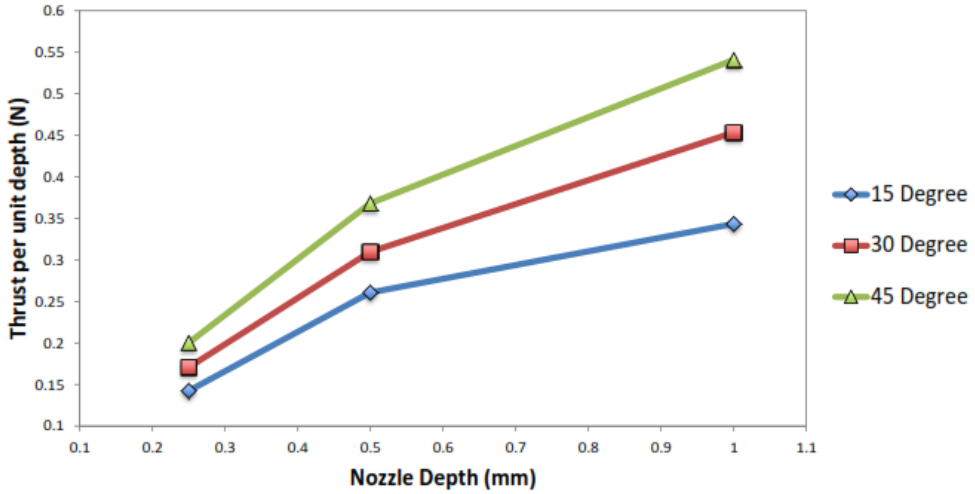

Figure B.5: The thrust performance per unit depth at Re ≈ 800 for 15°, 30° and 45° expander half-angles at 0.25, 0.50 and 1.00 mm. For the shallowest nozzles, the viscous boundary layer dominates the flowfield, which reduces performance.

Bibliography

[1] P. Panetta, H. Culver, J. Gagosian, M. Johnson, J. Kellogg, D. Mangus, T. Michalek, V. Sank, and S. Tompkins, *"NASA-GSFC Nano-Satellite Technology Development"*, 12th AIAA/USU Conference on Small Satellites, 1998.

[2] K. Lau, S. Lichten, L. Young, and B. Haines, *"An Innovative Deep Space Application of GPS Technology for Formation Flying Spacecraft"*, AIAA GN & C Conference, 1996.

[3] K. Carroll, H. Spencer, and R. Zee, *"CARAVEL: a solar-sail-based nanosatellite mission to a near-earth asteroid"*, 2012 Canadian Space Summit, 2012.

[4] M. Boucher, *"CARAVEL: A Solar-Sail-Based Nanosatellite Mission to a Near-Earth Asteroid"*, SpaceRef Canada, 2012.

[5] The CubeSat Program Cal Poly SLO, *"CubeSat Design Specification, REV 13"*, California Polytechnic State University, 2015.

[6] M. Swartwout, *"The First One Hundred CubeSats: A Statistical Look"*, Journal of Small Satellites, 2013.

[7] K. Kelley, *"Launch Systems to Support the Booming Nanosatellite Industry"*, Aerospace Conference, 2015 IEEE, 2015.

[8] S. Clark, *"Record-Setting 33 Tiny 'CubeSats' Launched From Space Station"*, Spaceflight Now, 2014.

[9] J. Mueller, R. Hofer, M. Paerker, and J. Ziemer. *"Survey of Propulsion Options for CubeSats"*, 57th JANNAF Propulsion Meeting, May 2010.

[10] NASA,*"NASAfacts, ELaNa XI CubeSat Launch on AFSPC-5"*,(2015).

[11] SpaceFlight101, *"Flock 1/2 - Planet Labs Earth Observation Satellites"*, Online: www.spaceflight101.com/flock/, 2015.

[12] NASA, Mission Design Division Staff. *"Small Spacecraft Technology State of the Art"*,(2014).

[13] S. Widdis, K. Asante, D. Hitt, M. Cross, W. Varhue, M. McDevitt, *"A MEMS-Based Catalytic Microreactor for a H_2O_2 Monopropellant Micropropulsion System"*, IEEE/ASME Transactions on Mechatronics, 2013.

[14] T. Yuan, and A. Li, *"Design and Fabrication of a MEMS-Based Millinewton Level Hydrazine Thruster"*, 45th AIAA/ASME/SAE/ASEE Joint Propulsion conference, 2009.

[15] D. Platt, *"A Monopropellant Milli-Newton Thruster System for Attitude Control of Nanosatellites"*, 16th Annual AIAA/USU Conference on Small Satellites, 2002.

[16] J. Dankanich, *"Small Satellite Propulsion"*, AstroRecon2015, 2015.

[17] C. Carpenter, D. Schmuland, J. Overly, and R. Masse, *"Test Results for the MPS-120 and MPS-130 CubeSat Propulsion Systems"*, Areojet Rocketdyne, 2014.

[18] C. Biddy, and T. Svitek, *"Monopropellant Micropropulsion System for CubeSats"*, 23rd Annual AIAA/USU Conference on Small Satellites, 2009.

[19] Tethers Unlimited Inc., "HYDROS Water Electrolysis Thruster Green Propellant, High-Thrust Propulsion for Orbit-Agile CubeSats", Online: http://www.tethers.com/HYDROS.html, Date Accessed: 04FEB2016.

[20] Vacco Industries, *"VACCO Delivers CubeSat Propulsion System for JPL Mars Cube One (MarCO)"*, Online: http://www.cubesat-propulsion.com/cubesat-propulsion-delivery, Date Accessed: 04FEB2016.

[21] Busek Co. Inc., *"Green Monopropellant Thrusters"*, Online: http://www.busek.com/index htm files/70008517C.pdf, Date Accessed: 04FEB2016.

[22] D. Hitt, C. Zakrzwski, and M. Thomas, *"MEMS-Based Satellite Micropropulsion via Catalyzed Hydrogen Peroxide Decomposition"*, Smart Materials and Structures, 2001.

[23] C. Kuan, G. Chen, and Y. Chao, *"Development and Ground Tests of a 100-Millinewton Hydrogen Peroxide Monopropellant Microthruster"*, Journal of Propulsion and Power, 2007.

[24] C. Kuan, G. Chen, and Y. Chao, *"Development of a High Test Hydrogen Peroxide (HTP) Micro-Thruster"*, 20th International Colloqium on the Dynamics of Explosions and Reactive Systems, 2005.

[25] J. Huh, and S. Kwon, *"Design, fabrication and thrust measurement of a micro liquid monopropellant thruster"*, Journal of Micromechanics and Microengineering, 2014.

[26] E. Wernimont, M. Ventura, G. Garboden, and P. Mullens, *"Past and Present Uses of Rocket Grade Hydrogen Peroxide"*, General Kinetics LLC, 1999.

[27] M. Jeff, *"Hydrogen Peroxide - The Safe Supply and Handling of HTP"*, Solvay Interox Inc, 2004.

[28] M. Ventura, E. Wernimont, S. Heister, and S. Yuan, *"Rocket Grade Hydrogen Peroxide (RGHP) for use in Propulsion and Power Devices - Historical Discussion of Hazards"*, 43rd AIAA/ASME/SAE/ASEE Joint Propulsion Conference & Exhibit, July 2007.

[29] M. Ventura, *"Long Term Storability of Hydrogen Peroxide"*, 41st AIAA/ASME/SAE/ASEE Joint Propulsion Conference & Exhibit, 2005.

[30] B. Halliwell, M. Clement, and L. Long, *"Hydrogen peroxide in the human body"*, Federation of European Biochemical Societies, 2000.

[31] Chemical and Material Sciences Department Research Division, Rocketdyne, *"Hydrogen Peroxide Handbook"*, Air Force Rocket Propulsion Laboratory Research and Technology Division, 29 August 1967.

[32] J. Rusek, *"Hydrogen Peroxide for Rocket Propulsion Applications"*, US Navy, 1995.

[33] J. Laat, and H. Gallard, *"Catalytic Decomposition of Hydrogen Peroxide by Fe(III) in Homogeneous Aqueous Solution: Mechanism and Kinetic Modeling"*, Environmental Science and Technology, 1999.

[34] A. Cervone, L. Torre, L. d'Agostino, A. Musker, G. Roberts, C. Bramanti, and G. Saccoccia, *"Development of Hydrogen Peroxide Monopropellant Rockets"*, AIAA Paper 5239, 2006.

[35] M. Gauer, D. Telitschkin, U. Gotzig, Y. Batonneau, H. Johansson, M. Ivanov, P. Palmer, and R. Wiegerink, *"First Results of PRECISE – Development of a MEMS-based monopropellant micro chemical propulsion system"*, Acta Astronautica, 2014.

[36] Dslauretta, *"Integration of the OSIRIS-REx Main Propellant Tank"*, DSLAURETTA Online: http://dslauretta.com/2014/12/16/integration-of-the-osiris-rex-main-propellant-tank/, 2014.

[37] K. Bedingfield, R. Leach, and M. Alexander, *"Spacecraft System Failures and Anomalies Attributed to the Natural Space Environment"*, NASA, 1996.

[38] M. McDevitt, and D. Hitt, *"Enhanced Homogeneous Catalysis in a Monopropellant Microthruster"*, Proc. AIAA SciTech 2015 Conference, 2015.

[39] D. Schmuland, C. Carpenter, R. Masse, and J. Overly, *"New Insights Into Additive Manufacturing Processes: Enabling Low-Cost, High-Impulse Propulsion Systems"*, 27th Annual AIAA/USU Conference on Small Satellites, 2013.

[40] M. Dushku, and P. Mueller, *"Additively Manufactured Propulsion System"*, 26th Annual AIAA/USU Conference on Small Satellites, 2012.

[41] C. Gutierrez, R. Salas, G. Hernandez, D. Muse, R. Olivas, E. MacDonald, M. Irwin, R. Wicker, M. Newton, K. Church, and B. Zufelt, *"CubeSat Fabrication*

through Additive Manufacturing and Micro-Dispensing", 7th International Conference and Exhibition on Device Packaging, 2011.

[42] W. Marshall, M. Zemba, C. Shemelya, R. Wicker, D. Espalin, E. MacDonald, C. Keif, and A. Kwas, *"Using Additive Manufacturing to Print a CubeSat Propulsion System"*, 51st AIAA/SAE/ASEE Joint Propulsion Conference, 2015.

[43] D. Espalin, D. Must, E. MacDonald, and R. Wicker, *"3D Printing Multifunctionality: Structures with electronics"*, International Journal of Advanced Manufacturing Technology, 2014.

[44] G. Moore, W. Holemans, A. Huang, J. Lee, M. McMullen, J. White, R. Twiggs, B. Malphrus, N. Fite, D. Klumpar, E. Mosleh, K. Mashburn, D. Wilt, J. Lyke, S. Davie, W. Bradly, T. Chiasson, J. Heberle, and P. Patterson, *"3D Printing and MEMS Propulsion for the RAMPART 2U Cubesat"*, 24th Annual AIAA/USU Conference on Small Satellites, 2010.

[45] D. Morris, and R. Noble, *"CubeSat Advanced Technology Propulsion System Concept"*, Aerojet Rocketdyne, 2014.

[46] T. Swanson, and T. Stephenson, *"Additive Manufacturing: Ensuring Quality for Spacecraft Applications"*, NASA, 2014.

[47] M. Qian, and F. Froes, *"Titanium Powder Metallurgy: Science, Technology and Applications"*, Butterworth-Heinemann, 2015.

[48] Little Giant (R), *"Chemical Resistance Chart"*, Online: http://www.usplastic.com/catalog/files/charts/LGCC.pdf, 2012.

[49] B. Horais, L. Love, R. Dehoff, *"The Use of Additive Manufacturing for Fabrication of Multi-Function Small Satellite Structures"*, 27th Annual AIAA/USU Conference on Small Satellites, 2013.

[50] W. Frazier, *"Metal Additive Manufacturing: A Review"*, Journal of Materials Engineering and Performance, 2014.

[51] T. Grunberger, and R. Domrose, *"Direct Metal Laser Sintering Identification of Process Phenomena by Optical In-process Monitoring"*, Laser Technik Journal, 2015.

[52] D. Gu, W. Meiners, K. Wissenbach, and R. Poprawe, *"Laser Additive Manufacturing of Metallic Components: Materials, Processes and Mechanisms"*, International Materials Reviews, 2012, Vol 57, No 3, 133-163.

[53] O. Nyrhila, A. Danzig, and M. Frey, *"Direct Metal Laser Sintering (DMLS) of Titanium Alloys"*, Electro Optical Systems, 2010.

[54] L. Murr, S. Quinones, S. Gaytan, M. Lopez, A. Rodela, E. Martinez, D. Hernandez, E. Martinez, F. Medina, and R. Wicker, *"Microstructure and mechanical behavior of Ti-6Al-4V produced by rapid-layer manufacturing, for biomedical applications"*, Journal of the Mechanical Behavior of Biomedical Materials, 2009.

[55] F. Haber and J. Weiss, *"The Catalytic Decomposition of Hydrogen Peroxide by Iron salts"*, Proceeding of the Royal Society of London Series A, Mathematical and Physical Sciences, 1934.

[56] D. Keese, B. Melof, B. Ingram, W. Escapule, M. Grubelich, and J. Ruffner, *"Hydrogen Peroxide-Based Propulsion and Power Systems"*, Sania National Laboratories, April 2004.

[57] W. Kwan, and B. Voelker, *"Decomposition of Hydrogen Peroxide and Organic Compounds in the Presence of Dissolved Iron and Ferrihydrite"*, Environmental Science and Technology, 2002.

[58] A. Musker, G. Roberts, R. Horabin, A. Kawar, M. Payne, M. Pollard, and C. Ryan, *"An Assessment of Homogeneous Catalysts for the Rapid Decomposition of Hydrogen Peroxide"*, 42nd AIAA/ASME.SAE/ASEE Joint Propulsion Conference & Exhibit, 2006.

[59] S. Davis, and N. Yilmaz, *"Advances in Hypergolic Propellants: Ignition, Hydrazine, and Hydrogen Peroxide Research"*, Advances in Aerospace Engineering, 15 September 2014.

[60] B. Greenfield, W. Louisos, and D. Hitt, *"Numerical Simulations of Multiphase Flow in Supersonic Micro-Nozzles"*, 49th AIAA Aerospace Sciences Metting, 2011.

[61] J. Bradley, and A. Lang, *"Solubility Prediction in Any Solvent"*, Open Notebook Science, Online: http://showme.physics.drexel.edu/onsc/models/multisolvent.php, 2009.

[62] Arcos Organics, *"n-Hexane MSDS"*, Fisher Scientific, 2014.

[63] *"Compound Summary for CID 8103"*, PubChem, 2016.

[64] Sigma-Aldrich, *"2-Propanol MSDS"*, Sigma-Aldrich, 2016.

[65] Sigma-Aldrich, *"Methanol MSDS"*, Sigma-Aldrich, 2016.

[66] Sigma-Aldrich, *"Ethyl alcohol, pure MSDS"*, Sigma-Aldrich, 2016.

[67] W. Louisos, and D. Hitt, *"Viscous Effects on Performance of Three-Dimensional Supersonic MicroNozzles"*, J. Spacecraft & Rockets, 2012.

[68] A. Alfano, J. Mills, and G. Vaghjiani, *"Highly accurate ignition delay apparatus for hypergolic fuel research"*, Review of Scientific Instruments, 2006.

[69] B. Melof, and M. Grubelich, *"Investivation of Hypergolic Fuels with Hydrogen Peroxide"*, American Institute of Aeronautics & Astronautics, 2001.

[70] J. Blevins, R. Gostowski, and S. Chianese, *"An Experimental Investigation of Hypergolic Ignition Delay of Hydrogen Peroxide with Fuel Mixtures"*, AIAA, 2004.

[71] W. Louisos, A. Alexeenko, D. Hitt, and A. Zilic, *"Design Considerations for Supersonic Micronozzles"*, Int. J. Manufacturing Research, 2008.

[72] NASA, *"Schlieren System"*, Online: https://www.grc.nasa.gov/www/k-12/airplane/tunvschlrn.html, Date Accessed: 10FEB2016.

[73] L. Weinstein, *"Review and update of lens and grid schlieren and motion camera schlieren"*, Eur. Phys. J. Special Topics, 2010.

[74] H. Stone, A. Stroock, and A. Ajdari, *"Engineering Flows in Small Devices: Microfluidics Toward a Lab-on-a-Chip"*, Annual Review of Fluid Mechanics, 2004.

[75] A. Stroock, S. Dertinger, A. Ajdari, I. Mezic, H. Stone, and G. Whitesides, *"Chaotic Mixer for Microchannels"*, ScienceMag, 2002.